

ANODIZATION OF TITANIUM ALLOYS FOR ORTHOPEDIC APPLICATIONS

A THESIS SUBMITTED TO  
THE GRADUATE SCHOOL OF NATURAL AND APPLIED SCIENCES  
OF  
MIDDLE EAST TECHNICAL UNIVERSITY

BY

MERVE İZMİR

IN PARTIAL FULFILLMENT OF THE REQUIREMENTS  
FOR  
THE DEGREE OF MASTER OF SCIENCE  
IN  
METALLURGICAL AND MATERIALS ENGINEERING

JUNE 2018



Approval of the thesis:

**ANODIZATION OF TITANIUM ALLOYS FOR ORTHOPEDIC APPLICATIONS**

submitted by **MERVE İZMİR** in partial fulfillment of the requirements for the degree of **Master of Science in Metallurgical and Materials Engineering Department, Middle East Technical University** by,

Prof. Dr. Halil Kalıpçılar  
Dean, **Graduate School of Natural and Applied Science**

\_\_\_\_\_

Prof. Dr. Hakan Gür  
Head of Department, **Metallurgical and Materials Eng.**

\_\_\_\_\_

Assist. Prof. Dr. Batur Ercan

\_\_\_\_\_

Supervisor, **Metallurgical and Materials Eng. Dept., METU**

**Examining Committee Members:**

Prof. Dr. İshak Karakaya  
Metallurgical and Materials Eng. Dept., METU

\_\_\_\_\_

Assist. Prof. Dr. Batur Ercan  
Metallurgical and Materials Eng. Dept., METU

\_\_\_\_\_

Prof. Dr. Abdullah Öztürk  
Metallurgical and Materials Eng. Dept., METU

\_\_\_\_\_

Doç. Dr. Sedat Odabaş  
Chemistry Dept., Ankara University

\_\_\_\_\_

Assist. Prof. Dr. Sezer Özerinç  
Mechanical Engineering Dept., METU

\_\_\_\_\_

**Date:** 26.06.2018

**I hereby declare that all information in this document has been obtained and presented in accordance with academic rules and ethical conduct. I also declare that, as required by these rules and conduct, I have fully cited and referenced all material and results that are not original to this work.**

Name, Last name : Merve İzmir

Signature :

## **ABSTRACT**

# **ANODIZATION OF TITANIUM ALLOYS FOR ORTHOPEDIC APPLICATIONS**

İzmir, Merve

M.Sc., Department of Metallurgical and Materials Engineering

Supervisor: Assist. Prof. Dr. Batur Ercan

June 2018, 90 pages

In recent years, nanostructured oxide films on titanium alloy surfaces have gained significant interest due to their electrical, catalytic and biological properties, leading to an extensive effort to engineer nanostructured oxide films on titanium and titanium alloy surfaces. In literature, there is a variety of different approaches to fabricate nanostructured oxide films, including hydrothermal treatment, sol-gel synthesis, physical vapor deposition, electrodeposition, and etc. Among these methods, electrochemical fabrication processes have widely been explored due to their flexibility to control surface morphology at the micronscale and nanoscale. Anodization technique, which allows fine-tuning of oxide film thickness, feature size, topography and chemistry, is the most popular electrochemical approach to fabricate nanostructured oxide films on titanium alloys, and has been investigated for orthopedic and biomedical applications by multiple research groups. Briefly, anodization is the growth of a controlled oxide film on the surface of a metallic component attached to the anode of an electrochemical cell. This thesis explores the use of anodization of titanium alloys for orthopedic applications.

In this thesis, micropit structures were grown on Ti6Al4V surfaces via anodization using fluoride free electrolytes consisting of NH<sub>4</sub>Cl in distilled water. Furthermore, nanotubular structures were fabricated via anodization of Ti6Al7Nb surfaces in fluoride electrolyte. Fabricated surface structures were characterized for their physical and chemical properties and the bioactivity of the surfaces were determined by soaking samples in simulated body fluid up to 30 days. The thesis concludes with areas requiring further research to successfully translate anodized titanium alloys to clinics for orthopedic applications.

**Keywords:** Ti6Al4V, Ti6Al7Nb, anodization, topography, surface features, orthopedics.

## ÖZ

### TİTANYUM ALAŞIMLARININ ORTOPEDİ UYGULAMALARI İÇİN ANODİZASYONU

İzmir, Merve

Yüksek Lisans, Metalurji ve Malzeme Mühendisliği Bölümü

Tez Yöneticisi: Dr. Öğr. Üyesi Batur Ercan

Haziran 2018, 90 sayfa

Son yıllarda titanyum alaşımı yüzeyleri üzerindeki nanoyapılı oksit filmlerin oluşturulması için büyük çaba sarf edilmesi, nanoyapılı oksit filmlerin elektriksel, katalitik ve biyolojik özelliklerinden dolayı büyük ilgi görmüştür. Literatürde, hidrotermal methodu, sol-jel sentezi, fiziki buhar biriktirme, elektrodpozisyon, vb. yöntemleri olmak üzere nanoyapılı oksit filmleri üretmek için farklı yaklaşımlar vardır. Bu yöntemler arasında, elektrokimyasal üretim yöntemleri, mikron ve nanoboyutta oluşturulan yüzey morfolojisini kontrol etmeyi esnek kılmasından dolayı geniş çapta araştırılmıştır. Oksit film kalınlığının, çapların, yüzey topografi ve kimyasının kontrolünü mümkün kılan anodizasyon yöntemi, titanyum alaşımları üzerinde nanoyapılı oksit filmlerin üretilmesi için en popüler elektrokimyasal yaklaşım ve birçok araştırma grubu tarafından ortopedik ve biyomedikal uygulamalar için araştırılmıştır. Kısaca anodizasyon, bir elektrokimyasal cihazın anoduna bağlı metalik bir bileşenin yüzeyi üzerindeki kontrollü bir oksit filmin büyümesidir. Bu tez titanyum alaşımlarının ortopedi alanında kullanımı için anodizasyonunu araştırmaktadır.

Bu tez çalışmasında, damıtılmış su içinde  $\text{NH}_4\text{Cl}$  içeren florür içermeyen elektrolitlerde  $\text{Ti6Al4V}$  yüzeylerinin anodizasyonu kullanılarak mikropit yapılar üretilmiştir. Ayrıca, florit elektrolit içerisindeki  $\text{Ti6Al7Nb}$  yüzeylerinin anodizasyonu ile nanotübüler yapılar üretilmiştir. Üretilen yapıların fiziksel ve kimyasal özellikleri ve bu yüzeylerin biyoaktiviteleri 30 gün boyunca simüle edilmiş vücut sıvısı içerisinde tutularak belirlenmiştir. Tez, anodize titanyum alaşımlarının ortopedik uygulamaları başarılı bir şekilde kliniklere çevirmek için daha fazla araştırmaya ihtiyaç duyan alanlar ile sonuçlanacaktır.

**Anahtar Sözcükler:**  $\text{Ti6Al4V}$ ,  $\text{Ti6Al7Nb}$ , anodizasyon, topografi, yüzey özellikleri, ortopedi.



*To*

*My Dear Parents, Őengül &Hüsnü & Necmi*

*My Endless Love, Tuęba and Kübra*

*Your love, belief and support made this possible...*

## ACKNOWLEDGEMENTS

I would like to express my deep and sincere gratitude to everybody for their help and support throughout this research. First and most importantly, I would like to thank to my thesis advisor Assist. Prof. Dr. Batur Ercan not only for guidance and encouragement, but also his friendly attitude.

I would like to express my deep thanks to Prof. Dr. İbrahim Günal for supporting my academic life in terms of his ideas and guiding and supervising me for 4 years. I would like to express my sincere gratitude to Prof. Dr. Mehmet Parlak for providing opportunity to meet materials exciting world.

It was a privilege for me to work with these professors at METU.

This work was financially supported by METU Research Foundations (Grant No. BAP-08-11-2017-019) and The Scientific and Technological Research Council of Turkey (TÜBİTAK) grant number 117M187.

I would like to thank METU Biomaterials and Nanomedicine Laboratory current members for their help in experiment parts and creating peaceful environments on the lab. I am also thankful to Arif Aygündüz for the support and belief in my ideas and providing financial support for MRS 2017 Fall Meeting. I collected so good memories at Boston, thanks to my grandpa, Arif Aygündüz. Special thanks to Tuğba Ocakoğlu and Kübra Dal, for their excellent friendship and also their belief to me. I would like to express deep thanks to Süleyman Kanberoğlu for his being excellent friend, Asım Doğan Namlı for expert in my computer malfunction and being helpful friend, Arif Dönmez for being pretty mechanical guy, İdil Aygün for her being nice friend and all my other friends. In addition, I am also thankful to all METU Metallurgical and Materials Engineering Department technicians for their help in my experiments.

Finally, I want to express my deepest gratitude to my dear parents, İzmir family because they always support me. Besides, Tuğba Ocakoğlu and Kübra Dal behaved so kindly to me and their endless love and belief to succeed whatever I want made possible whatever I have achieved until today. Therefore, this study is dedicated to my family and my endless lovers.

## TABLE OF CONTENTS

ABSTRACT .....	vi
ÖZ .....	viii
ACKNOWLEDGEMENTS .....	xi
TABLE OF CONTENTS .....	xiii
LIST OF FIGURES .....	xv
CHAPTERS	
1. INTRODUCTION .....	1
1.1. Why Titanium and Titanium Alloys for Orthopedic Applications?.....	2
1.2. Mechanisms of Anodization.....	5
1.3. Anodization of Titanium and Titanium Alloys .....	10
1.4. <i>In vitro</i> studies investigated anodized titanium alloys .....	14
1.5. Research Objectives and Thesis Organization .....	21
2. FABRICATION OF MICROPIT STRUCTURES ON Ti6Al4V USING FLUORIDE FREE ANODIZATION .....	23

2.1. Experimental Details .....	25
2.1.1. Sample preparation.....	25
2.1.2. Preparation of Simulated Body Fluid.....	26
2.1.3. Surface Morphology.....	26
2.1.4. Surface Chemistry.....	26
2.1.5. Crystallinity .....	27
2.1.6. Mechanical Characterization.....	27
2.1.7. Water Contact Angle .....	27
2.2. Results and Discussion.....	28
2.3. Supporting Information: Fabrication of Micropit Structures Using Fluoride Free Anodization .....	40
3. INTERACTION OF ANODIZED Ti6Al7Nb WITH SIMULATED BODY FLUID .....	47
3.1. Experimental Details.....	48
3.1.1. Sample preparation.....	48
3.1.2. Preparation of Simulated Body Fluid.....	48
3.1.3. Surface Characterizations.....	48
3.2. Results and Discussion.....	49
4. CONCLUSION AND FUTURE WORK.....	57
REFERENCES.....	60

## LIST OF FIGURES

### FIGURES

Figure 1.1: Schematic depicting the growth of nanostructured oxide film on Ti6Al7Nb alloy.....	6
Figure 1.2: (a) Current density–time graph ( $j-t$ ) and (b) the representation of compact oxide layer (fluoride free electrolyte) and nanoporous/nanotubular oxide layers .....	8
Figure 1.3: SEM images showing nanotubular layers grown on (a) Ti6Al7Nb, (b) TiAl, and (c) TiZr using $(\text{NH}_4)_2\text{SO}_4$ electrolyte.....	12
Figure 1.4: (a), (b) and (c) SEM images of flower-like nanotubular structures on titanium at different magnifications.....	14
Figure 1.5: (a) Change of nanotubular diameters on titanium surfaces, (b) AFM scans showing the topography of conventional titanium and anodized nanotubular titanium having 40-60 nm diameters. ....	17
Figure 1.6: (a) Osteoblast densities on anodized surfaces up to 7 days of culture. (b) Influence of nanotubular diameter on osteoblast elongation,(c) focal contact formation of MSCs on 15 and 100 nm diameter nanotubular surfaces .....	19
Figure 2.1: Schematic of the set up used for anodization of Ti6Al4V samples in a fluoridefreeelectrolyte.....	25
Figure 2.2: (a), (b) and (c) SEM images and (d), (e) and (f) EDS spectra of Ti6Al4V, Anodized, Anodized-HT samples.....	30

Figure 2.3: FTIR spectra of Ti6Al4V (black line), Anodized (red line) and Anodized-HT (blue line) samples.....	31
Figure 2.4: XRD patterns of Ti6Al4V (black line), Anodized (red line) and Anodized-HT (blue line) samples.....	32
Figure 2.5: HR-TEM images of (a) Anodized and (b) Anodized-HT samples. Insets show SAED patterns obtained from these samples.....	33
Figure 2.6: XPS depth profiles of (a) Ti6Al4V, (b) Anodized and (c) Anodized-HT samples. ....	34
Figure 2.7: Sessile drop water contact angles of Ti6Al4V, Anodized and Anodized-HT samples.....	35
Figure 2.8: Microscratch test results showing (a) penetration depth vs. distance and (b) friction force vs. distance for Anodized samples.....	36
Figure 2.9: (a), (b) and (c) SEM images and (d), (e) and (f) EDS spectra of Ti6Al4V, Anodized and Anodized-HT samples immersed in 1x SBF for 30 days. ....	37
Figure S1: SEM images of Ti6Al4V samples anodized using 0.3 M NaCl electrolyte.....	40
Figure S2: SEM images of Ti6Al4V samples anodized using 3M HCl electrolyte.....	41
Figure S3: SEM images of Ti6Al4V samples anodized using 0.02 M HCl electrolyte.....	41
Figure S4: SEM images of Ti6Al4V samples anodized using 0.02 M HCl and 0.4 M NH <sub>4</sub> Cl electrolyte.....	42
Figure S5: SEM images of Ti6Al4V samples anodized using 0.2M NH <sub>4</sub> Cl electrolyte.....	43

Figure S6: SEM images of Ti6Al4V samples anodized using 0.4M NH <sub>4</sub> Cl electrolyte. .....	44
Figure S7: SEM images of Ti6Al4V samples anodized using 0.6M NH <sub>4</sub> Cl electrolyte.....	45
Figure S8: SEM cross sectional image of Anodized samples showing the approximate oxide layer thickness.....	46
Figure S9: (a), (b) and (c) SEM images and (d), (e) and (f) EDS spectra of Ti6Al4V, Anodized and Anodized-HT samples immersed in 1x SBF for 15 days. Insets show higher magnification images of samples.....	46
Figure 3.1: SEM images of a) Ti6Al7Nb-HT, b) Anod. 25-HT, c) Anod. 50-HT, d) Anod. 80-HT ve e) Anod. 140-HT samples. Scale bars are 3μm for lower magnification images and 500 nm for higher magnification images.....	50
Figure 3.2: Change of nanotubular diameters on Ti6Al7Nb samples with applied voltage. ....	51
Figure 3.3: a) Lower and b) higher magnification TEM images of the oxide layer formed on Ti6Al7Nb anodized at 20 V. ....	52
Figure 3.4 SEM images of Ti6Al7Nb alloys a), b) and c) before and d), e) and f) after 30-days exposure to simulated body fluid. .....	53
Figure 3.5: EDS spectra of a) Ti6Al7Nb-HT, b) Anod. 25-HT and c) Anod. 140-HT samples after 30 days exposure to SBF.....	54
Figure 3.6: FTIR spectra of Ti6Al7Nb surfaces after 30-day interaction with simulated body fluid. ....	55







## CHAPTER 1

### INTRODUCTION

The value of the global orthopedic implant market was USD 4.3 billion in 2015 and it is estimated to maintain a growth rate of 3% until 2020 [1]. Future projections indicate that in the U.S. alone, the number of total hip replacements will grow by 174% (572,000 procedures) and the number of total knee arthroplasties will grow by 673% (3.48 million procedures) by the end of 2030 [2]. The constantly rising geriatric population has primarily been driving the growth of orthopedic market since people aged above 65 years are at a high risk of developing orthopedic complications and about one out of every four 65-year-old person today is estimated to live past age 90 [3]. For the case total hip arthroplasty, considering the lifetime of a hip implant to be 15-20 years, most people having a hip replacement surgery require at least one revision surgery and multiple surgeries can be needed for younger more active patients [4, 5]. Clearly, implants with prolonged lifetime are required in orthopedic applications.

Currently, titanium and its alloys are widely used for fabrication of implants to replace hard tissue in orthopedics. Though orthopedic implants made of titanium alloys have been used in clinics for many years, limited lifetime of these implants has been a major issue, as stated in the previous paragraph. Integration of the implant with the juxtaposed bone tissue (osseointegration) has been one of the leading reasons for orthopedic implant failure. In fact, for hip replacement revision surgeries performed in the United States on November, 2017, implant failure rate due to osseointegration reached more than 25% [6].

Better integration of orthopedic implants with the surrounding bone tissue would improve implant stability and its lifetime, reducing the number of revision surgeries. To promote osseointegration of titanium based orthopedic implants, anodization method received specific attention due to its versatility creating nanophase topographies by tailoring the electrochemical parameters in the process. For instance, Zwilling *et al.* successfully fabricated self-organized array of nanotubes on titanium upon anodization [7]. In the following years, scientists observed improved bone cell functions *in vitro* and *in vivo* on these nanofeatured titanium oxide films, making anodized titanium alloys one of the promising materials in the orthopedic research field. Before providing an in-depth description of the anodization process and chemical mechanism of titanium anodization, the next section will briefly discuss the use of titanium and its alloys in the orthopedics field.

### **1.1. Why Titanium and Titanium Alloys for Orthopedic Applications?**

Titanium exhibits hexagonal close packed crystal structure at room temperature (HCP,  $\alpha$ -phase). As temperature of titanium is increased, it transforms to body centered cubic structure (BCC,  $\beta$ -phase) at beta transus (882.5°C) and eventually melt at 1678°C [8]. Titanium has excellent corrosion resistance, low density and high biocompatibility, making it the material of choice in orthopedic applications. However, bioinert nature of titanium, along with its suboptimal mechanical properties limit the lifetime of titanium based implants to 15-20 years [5]. To remedy these issues, titanium alloys have emerged as alternative implant materials. Titanium alloys can be categorized as  $\alpha$ , near- $\alpha$ ,  $\alpha+\beta$ , metastable  $\beta$  and stable  $\beta$  depending on their room temperature microstructures. Alloying elements incorporated into titanium are classified as three parts: i)  $\alpha$ -phase stabilizers (*i.e.* Al, O, N and C), ii)  $\beta$ -phase stabilizers (*i.e.* Mo, V, Nb, Ta, Fe, W, Cr, Si, Ni, Co, Mn and H) and iii) neutral alloying elements (*i.e.* Zr).  $\alpha$  and near- $\alpha$  titanium alloys show superior corrosion resistance, yet the ability to control their mechanical properties is limited due to their non-heat treatable nature to preserve  $\alpha$  phase microstructure. On the other hand,  $\beta$  titanium alloys can be shaped even at

lower temperatures because of its BCC crystal structure, making them ideal for complex geometries. Coupling the benefits of having both phases,  $\alpha + \beta$  titanium alloys exhibit higher tensile strength, fracture toughness, wear resistance and their heat treatable nature allows fabrication of complex geometries making them ideal for orthopedic implants [9, 10].

Among titanium alloys, Ti6Al4V based orthopedic implants have extensively been utilized to replace bone tissue in hip and knee replacements and bone fixation devices. Ti6Al4V has high strength and ductility and low density. In fact, strength of Ti6Al4V alloy can be increased with an increase in  $\beta$  stabilizer content, which further improves its fatigue limit. However, the major concern of using Ti6Al4V alloy in clinics is the presence of vanadium in its chemistry, which can potentially increase the expressions of pro-inflammatory factors, cause osteolysis, exhibiting toxic effect in the body [11]. Studies on biological response of metallic elements demonstrate that chemical composition of alloys used in biomaterial application, including orthopedic implants, must be optimized to limit adverse body reactions. Furthermore, there has been an extensive push by the regulatory bodies to direct manufacturers towards fabricating implants having minimum heavy metal content. Thus, alternative titanium alloys having different alloying elements and concentrations have been utilized towards improving the biocompatibility of the orthopedic implants. One such chemistry showing promise in patients is Ti6Al7Nb. Ti6Al7Nb has both  $\alpha$  and  $\beta$  phases, where aluminum stabilizes  $\alpha$  phase and niobium, replacing vanadium in Ti6Al4V alloy, stabilizes  $\beta$  phase. Ti6Al7Nb alloy is more ductile than Ti6Al4V, which permits easier fabrication into components having complex contours and has superior corrosion resistance compared to Ti6Al4V [12]. In fact, due to having superior corrosion resistance, mechanical strength and biocompatibility, Ti6Al7Nb alloy has gained significant popularity for femoral components of hip prostheses. Although incorporation of alloying elements into titanium's chemical composition as Al, V, Nb, and etc. satisfied some of the physical and chemical requirements to improve the lifetime of orthopedic implants, bioinert nature and the inability of titanium based

implants to integrate with the juxtaposed bone (osseointegration) is still a major concern and among the major reasons for orthopedic implant failure.

To enhance osseointegration of orthopedic implants, researchers modified the surfaces of implants which are in direct contact with bone tissue and demonstrated that when the implant surfaces provide a better environment for bone cell functions, integration of the implant with the juxtaposed bone tissue can be improved [13]. For this purpose, various surface modification techniques to alter physical and chemical properties of titanium alloy components have been investigated, *i.e.* hydrothermal treatment, sol-gel, sandblasting, physical and chemical vapor deposition, and etc. Among these techniques, anodization has been capturing the attention of multiple research groups for over a decade due to its simplicity, low cost and ability to control surface features at the nanoscale. In the anodization process, surface of a metallic component connected to the anode of an electrochemical cell is oxidized inside a suitable electrolyte, while an inert material, *i.e.* graphite or platinum, is used as the cathode. An electrical potential is applied between the electrodes to induce oxidation at the anode surface. In this process, electrochemical parameters, including anodization time, applied voltage, electrolyte composition and concentration, anodization temperature, and etc., can be controlled. By adjusting these electrochemical parameters, a nanostructured oxide film having an array of pits, wires, pores or tubes can be grown on the surface of the anode material and the dimensions of these surface features can be fine-tuned within the nanoregime.

Fabricating surface features having nanoscale dimensions is specifically important in tissue engineering where feature size of tissues is all in nanoregime. For instance, natural bone has inorganic constituent made up of 2-5 nm thickness and 20-25 nm wide hydroxyapatite crystals [14]. Another example is the vascular basement membrane which consists of a complex meshwork of pores and fibers in the submicron (100-1000nm) and nano (1-100nm) range [15]. By modifying biomaterial surfaces to possess features having nanophase topography, implant surfaces mimic the feature size

of natural tissues, providing a more realistic niche to promote cellular functions on implant surfaces. Since nanophase surface features similar to natural bone can be engineered upon anodizing titanium alloy surfaces, it provided researchers the rationale to investigate them in orthopedic applications. In the next chapter, the mechanism of anodization and formation of aforementioned nanophase surface features will be discussed.

## **1.2. Mechanisms of Anodization**

Anodization has been used to fabricate stable, protective and dense oxide layers on valve metals. Metals that can be anodized include aluminum, titanium, zinc, magnesium, zirconium, tantalum, hafnium, and etc., along with various alloys of these elements. Basically, anodization is the oxidation of these metals in certain electrolytes by generating an electrical field at metal/electrolyte interface. As stated previously, it is possible to fabricate nanofeatures having different morphologies and sizes on metallic surfaces via anodization. Fig. 1.1 shows schematic of the anodization process and different stages for nanotubular oxide formation on a Ti6Al7Nb alloy. Though this schematic indicates Ti6Al7Nb alloy as the anode, the mechanism of anodization is similar for all titanium alloys [16].

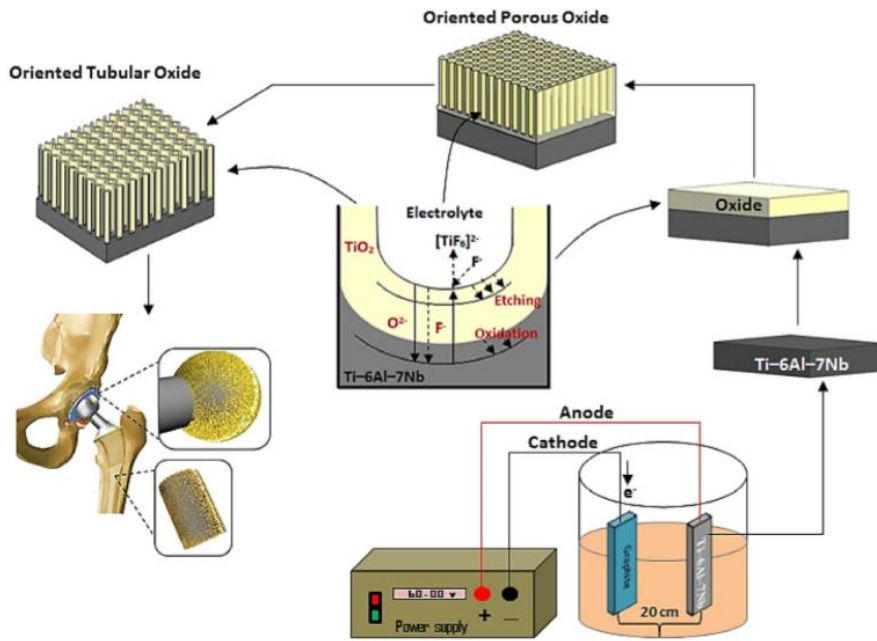
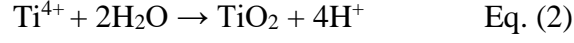


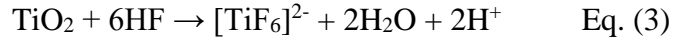
Figure 1.1: Schematic depicting the growth of nanostructured oxide film on Ti6Al7Nb alloy. Image is reprinted with permission from reference [16].

Basically, titanium and titanium alloys have a naturally occurring 2-5 nm thick passive oxide layer [17]. Electrical potential applied during anodization process increases the thickness of this natural oxide layer on titanium surfaces. Once voltage is applied to titanium alloys connected to the anode of an electrochemical cell, an oxidation reaction will start at the metal/metal oxide interface (Eq. (1)) and generate  $\text{Ti}^{4+}$  ions. These  $\text{Ti}^{4+}$  ions migrate outwards under the applied voltage, while  $\text{O}^{2-}$  ions present in the electrolyte migrate towards the metal/metal oxide interface. During migration of negatively charged  $\text{O}^{2-}$  ions towards the metal/metal oxide interface, they encounter  $\text{Ti}^{4+}$  ions ejected from the surface to produce a compact titanium oxide film (Eq.(2)). Due to having a higher electrical resistivity than the underlying titanium substrate, the applied voltage will decrease across the oxide film forming on the surface. During anodization, the oxide film will continue to grow as long as the electric field is strong enough to drive the ionic conduction across the oxide [18].





The formation of self-assembled nanostructures is generally associated with the presence of fluoride ions ( $\text{F}^-$ ) inside the electrolyte [19].  $\text{F}^-$  ions are small and capable of chemically reacting with the oxide layer, producing water-soluble metal fluoride complexes. In addition, these  $\text{F}^-$  ions can migrate inside the oxide film similar to  $\text{O}^{2-}$  ions. During anodization process, when titanium alloy at the anode is inserted inside the electrolyte, there is an immediate growth of oxide film on the surface of titanium alloy. When there are fluoride ions inside the electrolyte, pitting and decomposition of the compact oxide film occurs via Eq. (3), forming nanostructures on the titanium alloy surfaces.



As nanostructures (specifically nanotubes) grow, once a critical film thickness is reached, current density in the electrochemical cell stabilizes and the rate of oxide film growth at the titanium/titanium oxide interface and the rate of oxide film dissolution at the titanium oxide/electrolyte interface reach equilibrium. At this point, the oxide film does not get thicker any more, reaching its maximum thickness. It is important to realize that nanotubular structures on the surface will still continue to grow with oxide film steadily moving further into the titanium alloy, yet formation and dissolution rates are equal and thus prevent increase in oxide film thickness. Higher anodization voltages increase the oxidation and field-assisted dissolution, and thus provide oxide layers with different maximum layer thicknesses.

Depending on fluoride concentration of the electrolyte, three distinct morphology regimes can be obtained for the oxide film forming on titanium alloys. If the fluoride content is very low, a compact oxide film forms above a certain electrical

potential,  $U_p$  (passivation potential). If the fluoride concentration is at an intermediate level, nanoporous/nanotubular structures can be obtained and if the fluoride concentration is high, all the  $Ti^{4+}$  cations react with fluoride to form soluble  $[TiF_6]^{2-}$ , forming self-organized nanotubular layers. Having this said, current density-time curves obtained during anodization of titanium alloys (Fig. 1.2a) demonstrate different regimes, each of them corresponding to distinct oxide film morphology (Fig.1.2b). Specifically, in the first regime a compact oxide film is produced on titanium alloys, leading to a significant drop in the current density. In the second regime, there is an increase in current density, which is attributed to the formation of nanoporous structures in the oxide film. In the third and last regime, current density decreases gradually, indicating growth of nanoporous/nanotubular structure [20].

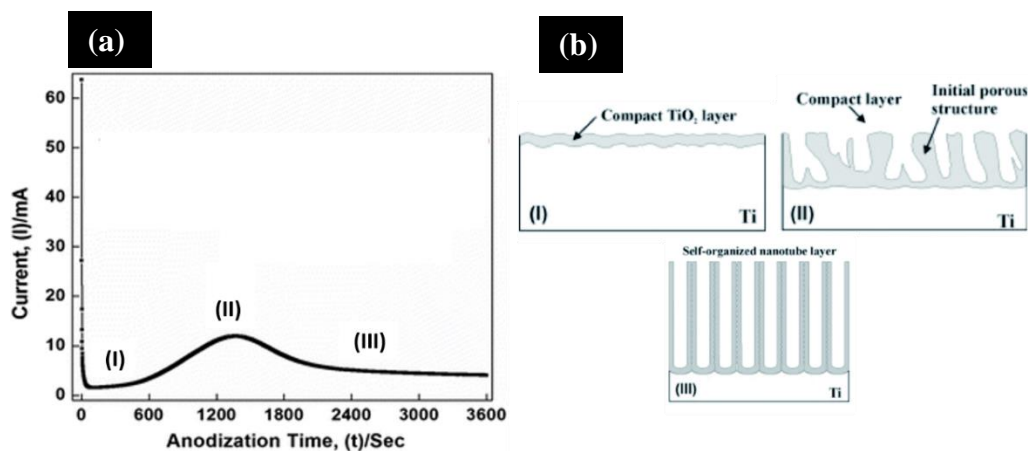


Figure 1.2: (a) Current density–time graph ( $j-t$ ) obtained during anodization of titanium using an electrolyte containing fluoride ions and (b) the representation of compact oxide layer (fluoride free electrolyte) and nanoporous/nanotubular oxide layers (fluoride containing electrolyte). Images are adapted with permission from reference [20, 21].

By tailoring the anodization parameters, i.e. electrolyte type, electrolyte concentration, pH, temperature, applied voltage and time, it is possible to control physical and chemical properties of the oxide film forming on the titanium alloys [22, 23, 24]. In literature, nanostructures in the form of compact oxide films, disordered porous films and self-organized porous and nanotubular films were fabricated by anodization using various electrolytes, i.e.  $\text{NH}_4\text{F}$ ,  $\text{CH}_3\text{COOH}$ ,  $\text{H}_2\text{SO}_4$ ,  $\text{HF}$ ,  $\text{Na}_2\text{HPO}_4$ ,  $\text{NaF}$ ,  $\text{NaOH}$ ,  $\text{NH}_4\text{Cl}$  and etc [25]. In addition, it is well-established that different electrolytes have different ionic conductivities, and thus form different electrical fields inside an electrochemical cell. When the electrical field is high, it will be easy to induce breakdown fields, which are localized on rough surfaces during the initial step of anodization. Furthermore, pH of the electrolyte is an important parameter to control growth and self-organization of nanotubular structures. For example, Feng et al. demonstrated using a  $\text{NH}_4\text{F}$ /water/glycerol electrolyte system that basic environment (pH 8-9) is much more efficient for self-organization of longer nanotubes than the commonly used acidic condition (pH 3-5) for titanium [26]. In another study, nanotubular formation rate was correlated with pH of the electrolyte where increase in pH of the electrolyte decreased nanotubular length [27]. Another parameter that control microstructure of the oxide film on titanium and titanium alloys is the temperature of electrolyte, which was found to effect dissolution rate of nanostructures [25]. It is interesting to note that while nanotubular diameters of oxide films do not depend on anodization temperature of aqueous electrolytes, they were found to increase with an increase in temperature once organic electrolytes. This phenomenon was explained with increasing electrolyte viscosity and decreasing ionic migration at lower temperature [28]. Applied voltage was another anodization parameter influencing surface microstructure, pore morphology, pore diameter, inter-pore distance and oxide film thickness forming on the titanium and titanium alloy substrates [29, 30]. As anodization voltage was increased, the web-like oxide surface morphology forming at lower voltages was lost and the microstructure of the oxide film gradually transform to nanotube like structures. Additionally,

duration of anodization alters nanotube morphology, increasing the oxide film thickness, while decreasing nanotubular wall thickness at longer anodization times [20]. To sum all these findings, during anodization of titanium and titanium alloys, changes in electrochemical process parameters alter growth kinetics, microstructure and formation of nanofeatures on the substrate surfaces, influencing the physical and chemical properties of the oxide film, which will be covered in the next section.

### **1.3. Anodization of Titanium and Titanium Alloys**

Early works on anodization of titanium were conducted in hydrofluoric and chromic acid containing electrolyte mixtures to enhance corrosion resistance of the underlying titanium without any consideration to fabricate a nanofeatured oxide film [31]. It was in 2003, Schumiki *et al.* reported fabrication of nanotubular structures using a mixture of sulfuric acid and small amounts of HF (0.15 wt %) [32]. In this study, they reported possibility of using alternative acid mixtures, *i.e.* phosphoric and acetic acid, in combination with HF or NH<sub>4</sub>F as potential electrolytes for anodization to fabricate nanoporous surface oxides. In another study, self-assembled nanotubular oxide films as thick as 500 nm was fabricated for the first time using a chromic acid containing electrolyte with and without incorporation of hydrofluoric acid [33]. Later on, Grimes *et al.* reported formation of nanotubular oxide having 4.4 μm length by anodizing titanium in a fluorinated solution having pH value of 4.5 [34]. Macak *et al.* confirmed previous findings and showed that pH of the electrolyte influence nanotubular length and oxide film thickness, where lower pH values restrict the length of nanotubes by enhancing the tube dissolution rate. They also showed that while smooth nanotubes without any surface ripples could be grown using non-aqueous electrolytes, fabrication of hexagonally arranged nanotubular layers could be grown using an organic electrolyte, *i.e.* ethylene glycol [35].

Anodization of titanium alloys used in orthopedic applications, *i.e.* Ti6Al4V and Ti6Al7Nb, has also been investigated. Macak *et al.* anodized both Ti6Al4V and Ti6Al7Nb in 0.5 wt% (NH<sub>4</sub>)<sub>2</sub>SO<sub>4</sub> + NH<sub>4</sub>F solution and successfully obtained self-assembled nanotubular oxide films on these substrates [28]. Since Ti6Al4V and Ti6Al7Nb are dual phase alloys, nanotube formation kinetics were found to be different for  $\alpha$  and  $\beta$  phases, where Mazare *et al.* reported earlier formation of nanotubular structures on  $\beta$  phase compared to  $\alpha$  phase for Ti6Al7Nb alloy using an aqueous electrolyte containing CH<sub>3</sub>COOH and 0.5 wt. % HF under 10 V potential [36]. Kaczmarek *et al.* observed changes in the morphology of nanotubular oxide films on  $\alpha$  and  $\beta$  phases depending on the fluoride concentrations used for the electrolyte [30]. In an extreme case, only  $\alpha$  phase exhibited nanotubular structures upon anodizing in 1M H<sub>3</sub>PO<sub>4</sub> and 0.2 wt. % HF electrolyte, while  $\beta$  phase did not form any nanostructures, indicative of different reactivities of each phase for fluoride containing electrolytes [37].

Park *et al.* examined the growth behavior of nanotubular oxide on Ti6Al4V substrates in glycerol containing electrolytes [38]. Anodized surfaces showed a wide distribution of nanotubular diameters, where nanotubes with smaller diameters formed across spaces present between nanotubes with larger diameters. Interestingly, diameters of the nanotubular features were increasing towards the base of the nanotubes as opposed to the commonly observed tapered nanotubular morphology. This study also highlighted the importance of electrolyte concentration used in anodization of titanium alloys, where diameters of the nanotubular features could be controlled by merely altering electrolyte concentration. Nanotubular features having 88.5 nm and 122.9 nm diameter were formed in glycerol electrolytes containing 1 wt. % NH<sub>4</sub>F + 20 wt.% H<sub>2</sub>O and 1 wt.% NH<sub>4</sub>F+ 30 wt.% H<sub>2</sub>O at 20 V, respectively [38]. Another method to control tubular diameters was altering anodization parameters. For instance, Mohan *et al.* formed self-assembled nanotubular oxide films having 35, 100 and 125 nm average tubular diameters on the Ti6Al7Nb alloy by adjusting the applied voltage to 10, 20 and 30 V, respectively [39].

In addition to Ti6Al4V and Ti6Al7Nb, self-assembled nanotubular structures have been reported for anodization of other titanium binary alloys, *i.e.* TiNb, TiZr, TiTa, TiW, TiMo and TiAl, as well as on ternary and more complex alloy systems of titanium. As expected, the morphology of nanotubular structures differed for each alloy despite having similar electrolytes (Fig. 1.3) [21].

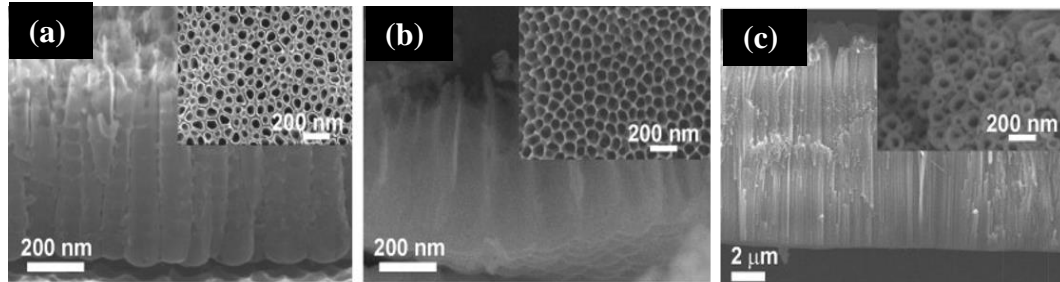


*Figure 1.3: SEM images showing nanotubular layers grown on (a) Ti6Al7Nb, (b) TiAl, and (c) TiZr using  $(\text{NH}_4)_2\text{SO}_4$  electrolyte. Larger images show cross-sectional views and insets show top views of nanotubular layers. Images are adapted with permission from reference [21].*

During anodization fluorinated electrolytes was often used for the fabrication of nanotubular structures on titanium and titanium alloys. However, few researchers reported chloride ions (another element found in the 7A group of the periodic table) to play a similar role during anodization [40]. Since chloride ions provide a less hazardous alternative to the highly toxic fluoride based electrolytes, various issues in industrial applications can be avoided, *i.e.* corrosion, toxicity, environmental influence and etc. Researchers observed that chloride containing electrolytes in combination with perchloric, oxalic or formic acid was successful in fabricating nanotubular surfaces on titanium, as seen Fig. 1.4. Although the mechanism of anodization using chlorinated electrolytes was not clear, pits appear on titanium surfaces, as shown in the Fig. 1.4a, b and c followed by rapid formation of nanotubular arrays inside the pits.

The corresponding current-time graph upon applying 10V potential using 0.5M HCl aqueous electrolyte is consistent with the graph shown in Fig.1.2 [41]. However, nanotubular arrays formed via fluoride free anodization were inhomogeneous and disordered, not fully covering the titanium surfaces. Additionally, using fluoride free anodization, nanotubular features having diameters as small as 20 nm could be fabricated, while carbon contamination over 20% was found over the oxide films in several chlorine based electrolyte systems, *i.e.* 0.4M NH<sub>4</sub>Cl+0.5M formic acid, 0.4M NH<sub>4</sub>Cl+0.05M sulfuric acid and 0.4M NH<sub>4</sub>Cl+0.5M formic acid electrolytes [25, 40]. Having this said, the role of other chemicals typically used in fluorinated electrolytes, *i.e.* ethylene glycol, for anodization of titanium and titanium based alloys in chloride based electrolytes is not clear and could be a key component to obtain uniformly distributed nanotubular features for chlorine based electrolyte systems. For the case of titanium anodization using halogen-free electrolytes, Kim *et al.* suggested rapid breakdown mechanism, which is basically the local breakdown of oxide film by ions, for growth of nanotubular bundles [42]. Perhaps altering the anodization conditions which influence rapid breakdown anodization mechanism, *i.e.* applied potential, water content, chloride and other ion concentrations, may lead to formation of self-organized nanotubular structures in both fluoride-free and halogen-free electrolytes [25]. Further research is required on fluoride-free and halogen-free anodization to identify formation mechanism of nanotubes and to obtain homogenous surface distribution.

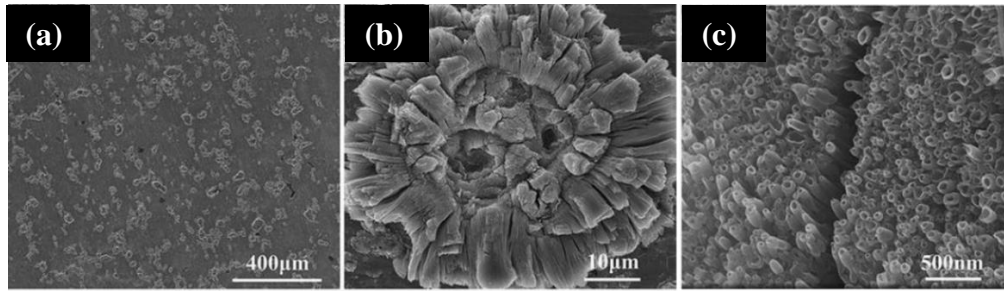


*Figure 1.4: (a), (b) and (c) SEM images of flower-like nanotubular structures on titanium at different magnifications. Titanium samples were anodized using an electrolyte containing 0.3 M sodium chloride and 6:4 distilled water to ethylene glycol ratio. Images are adapted with permission from reference [43].*

#### **1.4. *In vitro* studies investigated anodized titanium alloys**

In the orthopedics field, preventing implant failure is the ultimate challenge. To accomplish this aim, enhancing adhesion, proliferation and cellular functions of bone cells on currently used titanium based implants, and thus improving osseointegration of the implant is an important necessity. Since cellular functions are mediated by physical and chemical properties of the surface they interact with, bone cell-implant interface has been the focus of many studies [44].

When an orthopedic implant is inserted into the body, proteins in the plasma and the surrounding tissues adsorb onto the implant surfaces within the first couple of seconds. Depending on the surface properties of the implant, concentration and confirmation of the adsorbed proteins can significantly differ. Specifically, implant surface chemistry, energy, topography, crystallinity, texture, and etc. influence adsorption of proteins onto its surfaces. Since adsorbed proteins play a key role mediating cellular functions for anchorage dependent cells, aforementioned surface properties of orthopedic implants have a major influence on how implant interacts with juxtaposed bone tissue, osseointegration and long-term success of the implant. The main mechanism of bone cell adhesion onto implant surfaces is



the interaction of cell membrane receptors, called integrins, with RGD (R: arginine, G:glycine, D: aspartic acid) peptide sequence of the adsorbed proteins. The proteins in the blood plasma that have RGD peptide sequence are fibronectin, vitronectin, laminin and collagen, and their adsorption onto orthopedic implant surfaces is the dominant mechanism controlling osteoblast (bone cell) adhesion onto implant surfaces.

Once surface of a biomaterial is fabricated to possess nanostructures, it exhibits completely altered physical and chemical properties compared to its conventional counterpart, and thus interact differently with serum proteins. In fact, this altered interaction with proteins results in enhanced biological properties for orthopedic applications. For instance, when surface of titanium samples was modified to possess nanophase surface roughness, enhanced fibronectin adsorption was observed compared to conventional titanium surfaces, altering adhesion of cells onto titanium surfaces [45]. Yao *et al.* reported 15% increase in both fibronectin adsorption and 18% increase in vitronectin adsorption on nanophase titanium structures compared to conventional titanium [46]. One of the pioneering works on interactions of osteoblasts with nanofeatured surfaces was reported by Webster *et al.* which showed increased osteoblast density, alkaline phosphatase activity and calcium deposition on nanophase alumina and titania compared to their conventional counterparts [47]. The same research group also reported that osteoblast adhesion, proliferation and long-term cellular functions were significantly improved on nanophase titanium, Ti6Al4V and CoCrMo alloys compared to their conventional counterparts having micron grain size [48]. In another study, nanophase titanium surface fabricated via electron beam evaporation showed enhanced osteoblast adhesion and cellular functions than conventional titanium surfaces [49]. Furthermore, nanostructured Ti6Al4V alloy prepared by severe plastic deformation supported increased osteoblast adhesion and expression of adhesion related integrin  $\beta 1$  gene on nano alloy compared with conventional samples. These results suggest that enhanced osteoblast cellular

function to nanophase surface topography is independent of the material type and controlled by the feature size of bone cell-material interphase [50].

Biological gains obtained by decreasing the surface feature size to nanoregime were also observed for anodized titanium and titanium alloys. Oh *et al.* showed enhanced interaction of osteoblasts with anodized titanium surfaces where filopodia of propagating osteoblasts were growing into nanostructured titanium oxide film and proposed it as an alternate mechanism for enhanced osteoblast functions on nanotubular titanium oxide surfaces [51]. Anodized Ti6Al4V surfaces promoted enhanced osteoblast densities, alkaline phosphatase activity and calcium deposition, which was correlated with greater vitronectin adsorption on anodized Ti6Al4V surfaces compared to its conventional counterpart [52]. Enhanced vitronectin adsorption was explained with increased hydrophilicity of Ti6Al4V alloy upon anodization, where sessile water drop contact angle measurements showed 60° for anodized samples, whereas it was 83° for the polished Ti6Al4V alloy [52]. These results were consistent with previous findings which demonstrated enhanced osteoblast functions on anodized nanotubular oxide samples compared to conventional titanium [53].

Recently, several research groups reported nanotubular feature size dependent changes in cellular functions for mesenchymal stem cells, hematopoietic stem cells, endothelial cells, osteoblast and osteoclast functions on anodized nanotubular titanium surfaces [54, 55]. The influence of nanotubular size was initially studied by Park *et al.* where self-assembled layers of vertically oriented nanotubular oxide films having 15 to 100 nm diameters were fabricated on titanium (Fig. 1.5) [56]. While the average surface roughness ( $R_a$ ) on conventional titanium substrates is nearly 6.54 nm, the surface roughness of anodized nanotubular samples was found to increase with increasing nanotubular diameter, reaching 12.62 nm for 40-60 nm diameter samples [57].

While the average surface roughness ( $R_a$ ) on conventional titanium substrates is nearly 6.54 nm, the surface roughness of anodized nanotubular samples was found to increase with increasing nanotubular diameter, reaching 12.62 nm for 40-60 nm diameter samples [57].

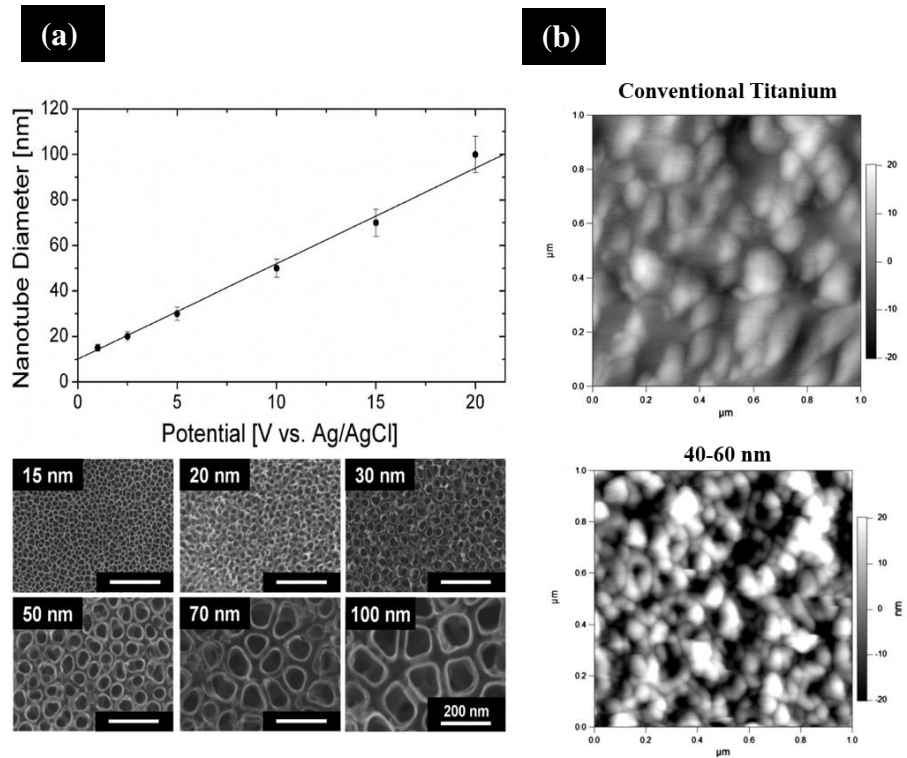


Figure 1.5: (a) Change of nanotubular diameters on titanium surfaces with the applied voltage and the corresponding SEM images of the anodized surfaces, (b) AFM scans showing the topography of conventional titanium and anodized nanotubular titanium having 40-60 nm diameters. Images are adapted with permission from reference [56, 57].

*In vitro* biocompatibility results showed mesenchymal stem cell adhesion, spreading, proliferation and osteogenic differentiation were all influenced by the diameter of nanotubular titanium oxide grown on titanium substrates. Specifically, mesenchymal stem cells density reached its highest value on nanotubular oxide

films having 15 nm diameter arrays [56]. Brammer *et al.* observed similar trends with osteoblasts, where nanotubular titanium samples having 30 nm diameter (the smallest diameter investigated in these studies) supported the highest cellular density compared to all other diameters after 2 days of culture (Fig. 1.6a) [58]. This study also confirmed elongation of osteoblasts with an increase in nanotubular diameter at 2 and 24 hours of culture (Fig. 1.6b). Yu *et al.* reported MC3T3-E1 preosteoblast behavior on anodized titanium oxide films with nanotubular diameters ranging between 20 nm to 120 nm [59]. Results showed well-spread cellular morphology on nanotubular samples having 20-70 nm diameters, while cellular adhesion and spreading was decreasing on samples having diameters larger than 70 nm. Similar results were obtained by Oh *et al.* who investigated the relationship between diameter of anodized nanotubular titanium and human mesenchymal stem cell (hMSC) morphology [60]. Their findings indicated that hMSCs on flat titanium appeared well-spread, while the ones on anodized samples having 100 nm nanotubular diameter expressed unidirectional lamellipodia extensions and filopodia after 2 hours of culture. After 24 hours, hMSCs began to demonstrate an elongated cellular morphology where aspect ratios of cells increased with an increase in nanotubular diameter. Park *et al.* studied the underlying mechanism for altered cellular response on nanotubular surfaces with different diameters and observed that nanotubes having 15 and 30 nm diameters elicited MSC response through extensive formation of paxillin-positive focal contacts which were anchored to actin stress fibers, while MSCs cultured on 100nm diameter nanotubular structures did not express distinct focal contacts (Fig. 1.6c) [56].

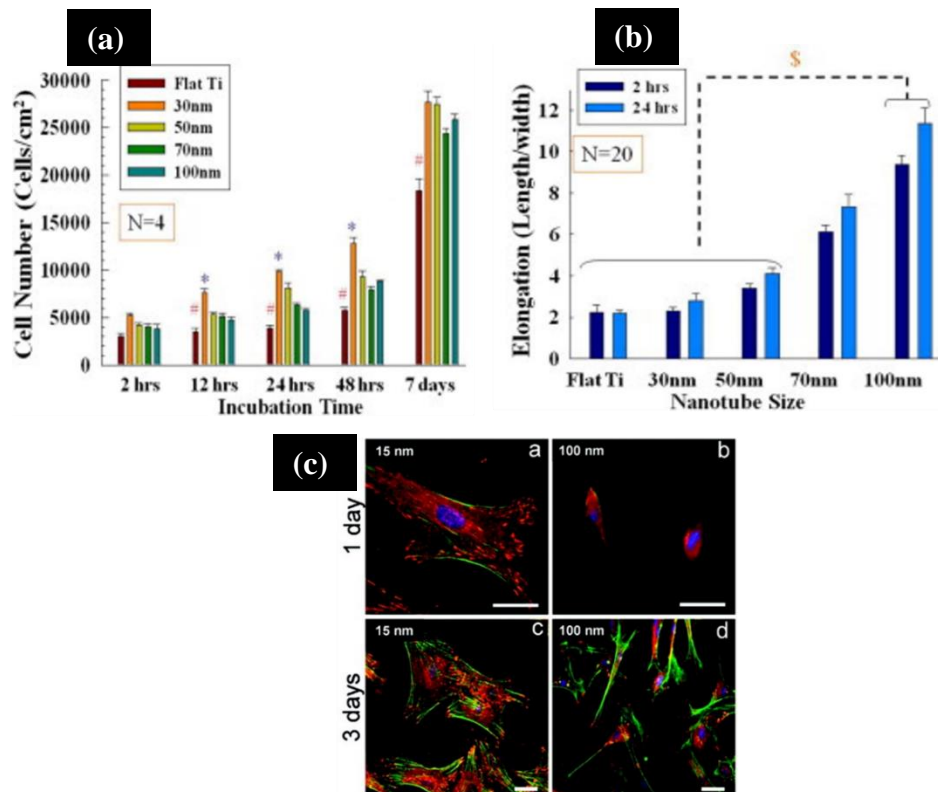


Figure 1.6: (a) Osteoblast densities on anodized surfaces up to 7 days of culture. # $p < 0.05$  indicates significant difference between the flat titanium and anodized nanotubular surfaces; \* $p < 0.05$  indicates significant difference between 30 nm diameter nanotubular features with larger size (50–100 nm) ones, (b) Influence of nanotubular diameter on osteoblast elongation, § $p < 0.05$  compared to flat titanium and 30 and 50 nm diameter nanotubular titanium. (c) focal contact formation of MSCs on 15 and 100 nm diameter nanotubular surfaces at 1 and 3 days of culture. Cells were stained for paxillin (red), actin (green) and nucleus (blue). Scale bars are a) and b) 50  $\mu\text{m}$  and c) and d) 100  $\mu\text{m}$ . Images are reprinted with permission from reference [56, 61].

Aside from cell density and morphology, nanotubular diameter of anodized titanium surfaces can also alter cellular functions. Malec *et al.* observed higher calcium deposition from human adipose tissue derived MSCs cultured on 108 nm diameter anodized nanotubular surfaces after 21 days of culture compared to untreated titanium

(S), electropolished titanium (W) and 80 nm diameter anodized nanotubular titanium surfaces [62]. Quantitative polymerase chain reaction (qPCR) analysis of osteocalcin (OCN), osteopontin (OPN) and alkaline phosphatase (ALP) gene expressions of hMSCs cultured for 14 days on anodized samples demonstrated regulation of these osteogenic genes on titanium samples having 70nm and 100nm diameter nanotubular features compared to cells cultured on other nanotubular diameters and conventional titanium. Importantly, in no osteogenic induction media was used in this study, highlighting the influence of surface nanofeature size on osteogenic differentiation of hMSCs.

In spite of the interesting *in vitro* biological response obtained from cells cultured on anodized nanotubular titanium surfaces with varying diameters, there are only a few studies testing the effect of nanotubular diameters for different titanium alloy formulations for orthopedic applications. Taylor *et al.* evaluated *in vitro* osteoblast response cultured on anodized Ti6Al7Nb alloy surfaces, where anodized nanotubular oxide films within 18 to 30 nm diameter range supported adhesion and proliferation of the osteoblasts up to 3 days of culture and maintained their integrity during *in vitro* cell experiments [63]. For the case of Ti6Al4V, anodized samples had higher SAOS-2 densities compared to glass controls. Nanotubular surfaces having larger average diameters had the highest concentrations of both vinculin and talin at 3 days of culture. Unlike anodized titanium samples, the highest concentrations of alkaline phosphatase, type I collagen and osteopontin were found on cells cultured on Ti6Al4V samples having smaller average nanotubular diameter [64]. Using a different cell line in this study could also contribute to the observed differences in literature.

It is important to stress that when titanium and titanium alloys are anodized to obtain nanotubular features with varying sizes, physical and chemical properties of the surfaces also change according to the electrochemical parameters used during anodization. For instance, root mean square roughness of the surface increases with an increase in nanotubular diameter, altering the hydrophobicity of the anodized surfaces,

and as a consequence, the interaction of the anodized surfaces with serum proteins, which controls adherent bone cell functions, is altered. Furthermore, chemical compositions of the surfaces also change depending on the anodization parameters since voltage driven migration of ions into the titanium lattice is altered. It is the combining all of these factors which influences interaction of cells with anodized surfaces. Controlling only one surface property without changing the rest via anodization is not possible. Thus, altered *in vitro* cellular response should not be only attributed to changes in feature size of nanotubes, instead a combination of multiple physical and chemical property changes come to play different roles. In fact, newly formed anodized surfaces can have very different surface properties compared to conventional titanium and titanium alloys that it is impossible to predict biological response merely from *in vitro* assays.

### **1.5. Research Objectives and Thesis Organization**

The main objectives of this research are:

1. Fabrication of micropit structures on Ti6Al4V surfaces via anodization using a fluoride-free electrolyte.
2. Fabrication of nanotubular structures via anodization of Ti6Al7Nb in fluoride containing electrolyte.
3. Characterization of the physical and chemical properties and the bioactivity of anodized samples by soaking them in simulated body fluid up to 30 days.

The organization of the thesis is given is summarized below:

This thesis consists of four main chapters to present the information covered in the study. Chapter 1 is separated into several parts to demonstrate a detailed literature about anodization and the use of anodized titanium alloys in orthopedics. In Chapter 2, the fabrication of micropit structures using fluoride-free electrolytes on anodized Ti6Al4V surfaces was investigated and bioactivity of these surfaces was assessed by soaking them in simulated body fluid for 30 days. In Chapter 3, fabrication of nanotubular surfaces via anodization of Ti6Al7Nb alloy using a fluoride containing electrolyte was investigated and bioactivity of nanotubular surfaces were again by soaking them in simulated body fluid for 30 days. Finally, Chapter 4 presents the conclusions derived from the results attained in this research and recommendations for the future work.



## CHAPTER 2

### FABRICATION OF MICROPIT STRUCTURES ON Ti6Al4V USING FLUORIDE FREE ANODIZATION

In literature, anodization of Ti6Al4V is typically investigated using fluorinated electrolytes to fabricate nanofeatured surfaces. For instance, Macak *et al.* anodized Ti6Al4V using an electrolyte mixture of 1M (NH<sub>4</sub>)<sub>2</sub>SO<sub>4</sub> + 0.5 wt% NH<sub>4</sub>F and the results demonstrated growth of self-organized porous oxide structures on Ti6Al4V surface [65]. Moreover, Park *et al.* also reported formation of nanotubular oxide on Ti6Al4V fixtures in 1wt% NH<sub>4</sub>F + glycerol + water containing electrolytes. Anodized surfaces of screws showed well-arranged and self-organized nanotubular titanium oxide layer [66]. Cumulatively, the use of fluorinated electrolytes lead to the formation of nanotubular structures on Ti6Al4V, which improved bone cell adhesion, proliferation and cellular functions *in vitro* compared to conventional Ti6Al4V [67]. However, the fragile nature of the nanotubular structures and weak delamination strength of the oxide based nanotubular coatings prevented translation of anodized nanotubular films from bench to bedside. Furthermore, the use of fluorinated electrolytes left behind fluoride based residues on anodized Ti6Al4V surfaces, which brought the risks of fluoride release from the anodized surfaces, which can potentially react with calcium mineral of the bone and red blood cells and lead to long term failure of implant. Thus, alternative anodization strategies to fabricate mechanically strong micro and nanofeatured surfaces without the use of fluorinated electrolytes on Ti6Al4V are required.

Few researchers reported possibility of using chloride containing electrolytes in combination with perchloric, oxalic or formic acid to anodize metallic surfaces and demonstrated chloride ions to play a similar role with fluoride during anodization [68]. It is important to note that chloride ions provide a less hazardous alternative to the highly toxic fluorinated electrolytes in industrial applications where the potential hazards can be corrosion, environmental influence, skin/lung exposure, etc [69]. Research showed that it was possible to obtain nanotubular structures having 20 nm diameter in various chlorine consisting electrolyte, *i.e.* 0.4M NH<sub>4</sub>Cl+0.5M formic acid, 0.4M NH<sub>4</sub>Cl+0.05M sulfuric acid and 0.4M NH<sub>4</sub>Cl+0.5M formic acid electrolytes [70, 71]. Aside from chloride containing electrolytes, various acid and salt solutions were also investigated as potential electrolytes. For instance, Cui *et al.* anodized Ti6Al4V in 1.0 M H<sub>2</sub>SO<sub>4</sub> solution at 150 V and 0.5 M Na<sub>2</sub>SO<sub>4</sub> solution at 100 and 130 V, followed by immersion in simulated body fluid for 7 days. The results showed deposition of calcium phosphate minerals on Ti6Al4V surfaces [72]. In another study, Narayanan *et al.* reported anodization of Ti6Al4V using a 0.3M phosphoric acid containing electrolyte where titanium oxide was obtained independent of the anodization duration [73]. However, the lack of biomimetic topography formation across Ti6Al4V surfaces and weak mechanical strength of the oxide films on anodized surfaces remain to be addressed to propose these anodization procedures for orthopedic applications.

This paper addresses the aforementioned issues, by introducing micropit structures that were fabricated on Ti6Al4V alloy surfaces using a fluoride-free electrolyte (NH<sub>4</sub>Cl aqueous solution) in anodization. Surface chemical composition, wettability, crystallinity and delamination resistance of the micropit structures were investigated. Lastly, bioactivity of the anodized micropit structures was also evaluated using simulated body fluid up to 30 days. This study provides a detailed fabrication route to form micropit surface topography on Ti6Al4V alloy surfaces and shows preliminary data supporting its potential use for orthopedic applications.

## 2.1. Experimental Details

### 2.1.1. Sample preparation

Ti6Al4V alloy rod (ASTM F136) was cut into 1 mm thick pieces using a precision cutter (Buehler, Linear Precision Saw). Obtained pieces were sonicated with acetone, ethanol (96% Pur. Gr.) and ultrapure water for 20 minutes, respectively. The cleaned Ti6Al4V samples were anodized using the anodization apparatus shown in Fig. 2.1. In this experiment, the platinum mesh (Alfa Aesar) is used as the cathode and the cleaned Ti6Al4V samples are used as the anode. The platinum mesh and Ti6Al4V samples were connected to a direct current (DC) power supply (TDK-Lambda Genesys 300V / 5A) via copper wire, and 0.4 M  $\text{NH}_4\text{Cl}$  was used as the electrolyte as seen Fig. 2.1. During the anodization process, the applied voltage was 30V for 2 minutes and the electrolyte solution was magnetically stirred. Once anodization is complete, followed by the anodized samples were rinsed with ultrapure water and dried at room temperature, followed by heat treatment at 500°C for 2 hours. In this study, control samples, anodized samples and heat treatment samples were denoted as Ti6Al4V, Anodized and Anodized-HT, respectively.

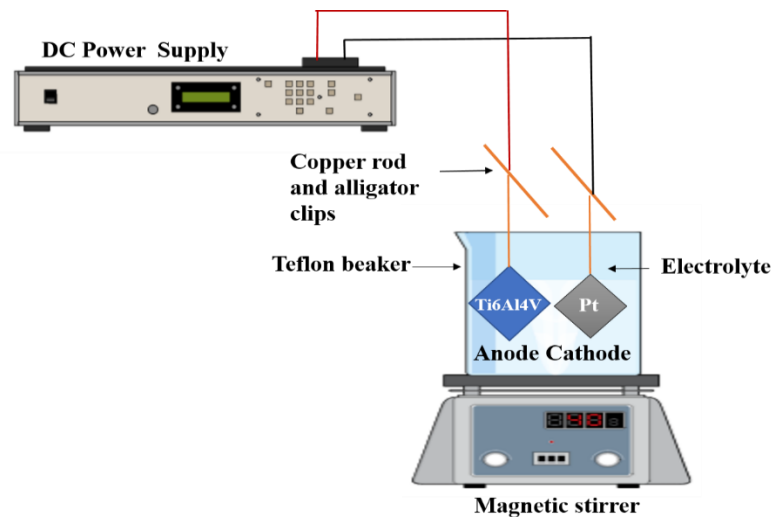


*Figure 2.1: Schematic of the set up used for anodization of Ti6Al4V samples in a fluoride free electrolyte.*

### **2.1.2. Preparation of Simulated Body Fluid**

Ti6Al4V, Anodized and Anodized-HT samples were soaked in simulated body fluid (SBF) up to for 30 days, maintained at 37 °C with pH 7.4. Reagents of simulated body fluid (SBF) were dissolved in the sequence of NaCl (8,035 g/L), NaHCO<sub>3</sub> (0,355 g/L), KCl (0,225 g/L), K<sub>2</sub>HPO<sub>4</sub> · 3H<sub>2</sub>O (0,231 g/L), MgCl<sub>2</sub> · 6H<sub>2</sub>O (0,311 g/L), 1 M HCl (39 ml), CaCl<sub>2</sub> (0,292 g/L), Na<sub>2</sub>SO<sub>4</sub> (0,072 g/L). Then, the solution was then buffered with Tris (6.118 g/L) and 1 M HCl [74]. Once SBF is prepared, Ti6Al4V, Anodized and Anodized-HT samples were immersed in SBF up to 30 days at 37 °C.

### **2.1.3. Surface Morphology**

Samples were characterized using scanning electron microscope (FESEM FEI NOVA NANO 430) to observe their surface morphology. 20 kV accelerating voltages was used to image samples. No coatings were used to image the surfaces. Three experiments were made on triplicate images for each sample group.

### **2.1.4. Surface Chemistry**

The chemical composition of samples was determined through energy dispersive spectroscopy using an EDAX-AMETEK detector in conjunction with scanning electron microscope.

Molecular bonds of Ti6Al4V alloy were characterized by Fourier Transform Infrared (FTIR) reflection spectroscopy (FTIR, Perkin Elmer 400) using attenuated total reflection (ATR) configuration. The spectra were collected in the 400–1100 cm<sup>-1</sup> range, with a resolution of 4.00 cm<sup>-1</sup>. The background spectra were subtracted from the obtained reflectance. For each sample, average of two spectra from different fields of each sample was reported.

For chemical profiling of the specimens, XPS was used to make Depth Profile Analysis. The specimens were scanned and the spectrum data were collected after each

sputtering (by Ar<sup>1+</sup> sputtering for 2 min), repeated five times in all to analyze the variation of elements among layer.

### **2.1.5. Crystallinity**

Samples were structurally analyzed using X-ray diffractometer (Rigaku D/Max-2200 X-ray Diffraction Machine). Using Cu-K radiation ( $\lambda=1.54 \text{ \AA}$ ) using an energy of 30 mA and 40 kV, data was collected from 20° to 60° diffraction angles ( $2\theta$ ) were scanned at a scanning rate of 0.5°/min.

To observe the microstructural origin of Anodized and Anodized-HT samples, transmission electron microscopy (TEM, JEOL JEM 2100F) was used. Oxide based micropit structures were carefully separated out from the Ti6Al4V alloy, dispersed in ethanol, centrifuged for 1 hour and then transferred to copper grids for TEM. They were characterized in high-resolution (HR) and selected area electron diffraction (SAED) modes at 200 kV accelerating voltage. SAED pattern were collected from a circular area approximately 0.12  $\mu\text{m}$  in diameter.

### **2.1.6. Mechanical Characterization**

Anodized specimens were fixed on MicroScratch Tester (Anton Paar) and force was applied onto the sample starting from 0.05 to 2N with a rate of 0.2 N/min with an indenter tip, Berkovich indenter with having a 5 $\mu$  diameter tip was used to scratch through a 0.5 mm-long region. Two scratches were measured from one sample

### **2.1.7. Water Contact Angle**

Contact angles were measured using a drop shape analysis system (EasyDrop; KRÜSS GmbH, Hamburg, Germany). The contact angle from 3  $\mu\text{L}$  double distilled water droplets was measured 10 seconds after the drop contacted surfaces of Ti6Al4V, Anodized and Anodized-HT. Four samples from each group were measured in five times.

## 2.2. Results and Discussion

In this research, an oxide based surface having micron-sized surface topography was fabricated on Ti6Al4V samples to enhance bioactivity for orthopedic applications. A fluoride-free electrolyte was used to prevent formation of fluoride residues on Ti6Al4V surfaces and preclude potential toxicity concerns upon implantation of anodized Ti6Al4V samples into the bone tissue. To obtain micropit morphologies, hundreds of trials were completed using various combinations of electrolytes, voltages and durations. Some of the promising results were displayed in Fig. S1-S7. Since chloride ions were shown to form tubular structures for elemental titanium [75], the use of electrolytes containing chloride ions, including NaCl, HCl and NH<sub>4</sub>Cl aqueous solutions, as well as their combinations with and without different acids, was investigated in this study. The first electrolyte for anodization was chosen as 0.3 M NaCl and voltages up to 20V for 2 min were investigated. In literature, Fahim *et al.* studied anodization of pure titanium sheets using the same electrolyte under 20V and observed formation of vertically-oriented nanotubular titanium bundles [76]. However, the present research only showed micron sized surface features without forming any nanotubular features. When 3M HCl electrolyte was used for anodization (Fig. S2), micron sized surface features present in Fig. S1 were lost. This result contradicted that of Allam *et al.* who anodized titanium foils using a 3 M HCl aqueous electrolyte and applied a potential up to 13V to get nanotubular titanium oxide [77]. Since 3M HCl was a concentrated acidic solution, a more dilute electrolyte was investigated (Fig. S3). Upon using a more dilute electrolyte of 0.02M HCl, micron sized features reappeared on Ti6Al4V alloy surfaces at 30V up to 2 min of anodization. However, crack formations on the anodized surfaces prevented the use of 0.02M HCl electrolyte. When 0.4 M NH<sub>4</sub>Cl + 0.02 M HCl was used as an electrolyte (See Fig.S4), as reported by Panaitescu *et al.* [78], first promising results were obtained upon the application of 30V for 2 min. Since incorporation of NH<sub>4</sub>Cl had a positive effect on anodization to fabricate micropit surface topographies, a detailed investigation for the use of NH<sub>4</sub>Cl electrolyte, including concentration of NH<sub>4</sub>Cl, applied potential and duration of anodization, was completed (See Fig.S5, S6 and S7). For these analyses 0.2 M, 0.4 M and 0.6 M NH<sub>4</sub>Cl electrolytes were investigated under 10V, 20V and

30V anodization potentials at 1 min, 2 min and 3 min durations. Though micron phase surface topographies appeared in some of the investigated conditions, the use of 0.4 M  $\text{NH}_4\text{Cl}$  and application of 30V potential for 2 min was chosen for this study due to lack of crack formation and repeatedly obtaining micropit morphologies on Ti6Al4V surfaces. During optimization of anodization parameters, electrolytes containing  $\text{H}_2\text{O}_2$ , oxalic acid and sulfuric acid [77, 78] which promoted growth of nanotubes for different metals [76, 77], were also investigated. As mentioned previously, the present research did not obtain tubular features using these electrolytes. We suspect that the use of different anode materials (pure titanium vs. Ti6Al4V) having different elemental compositions and crystalline phases in these experiments could be the potential reason behind it. Since Ti6Al4V alloy consisted of aluminum rich alpha phase and vanadium rich beta phase, as opposed to pure titanium having only alpha phase, Ti6Al4V alloy had different reactivities towards the electrolyte compared to pure titanium. Furthermore, the lack of reported anodization parameters in some of these experiments (*i.e.* anodization temperature and distance between electrodes) would contribute to the observed differences. Having this said, morphological differences between alpha and beta phases were also not present in this study. However, differences between anodization kinetics and morphologies between alpha and beta phases were demonstrated in literature. For instance, Macak *et al.* demonstrated formation of homogeneous nanotubular structures on alpha phase, while beta phases dissolved completely during anodization upon using fluorinated electrolytes [79]. Uniform formation of micropit morphology on alpha and beta phase upon anodization was also due to similar etching rates of alpha and beta phase inside the electrolyte, as well as limited electrical field induced migration of large chloride ions inside Ti6Al4V matrix, in contrast to smaller fluoride ions, which would influence the dissolution kinetics of the oxide layer. It was worth mentioning that though there was no difference in morphology between alpha and beta phases, anodized surfaces had non-uniform distribution of micropits across the specimen surface, indicating localized initiation and formation of pits. It is well-known that the presence of chloride ions tends to induce pitting in many metals, which is specifically the case for pitting corrosion, and these pits nucleate at microscopic scales at localized active sites [80]. This

phenomenon was observed in this research and it was in accord with other publications anodizing different alloys using chloride containing electrolytes [76, 78].

The surface morphology of Ti6Al4V alloy, micropit structures formed on anodized Ti6Al4V (named Anodized) and heat treated anodized Ti6Al4V samples (named Anodized-HT) could be observed in Fig. 2.2. Anodized samples had micropits on their surfaces with approximately 2-3  $\mu\text{m}$  inner diameters. It was clear that annealing process at 500°C for 2 hours preserved micropit structures on anodized Ti6Al4V samples (Fig. 2.2c). EDS analysis displayed the chemical composition of the Ti6Al4V samples before and after anodization (Fig. 2.2d and e), as well as after heat treatment (Fig. 2f). The EDS spectra confirmed presence of Ti, Al and V elements for the non-anodized samples, and Cl<sup>-</sup> was present for the anodized samples independent of the heat treatment process. Presence of chloride on Ti6Al4V samples upon anodization was in agreement with previous reports where chlorinated electrolytes were used [81].

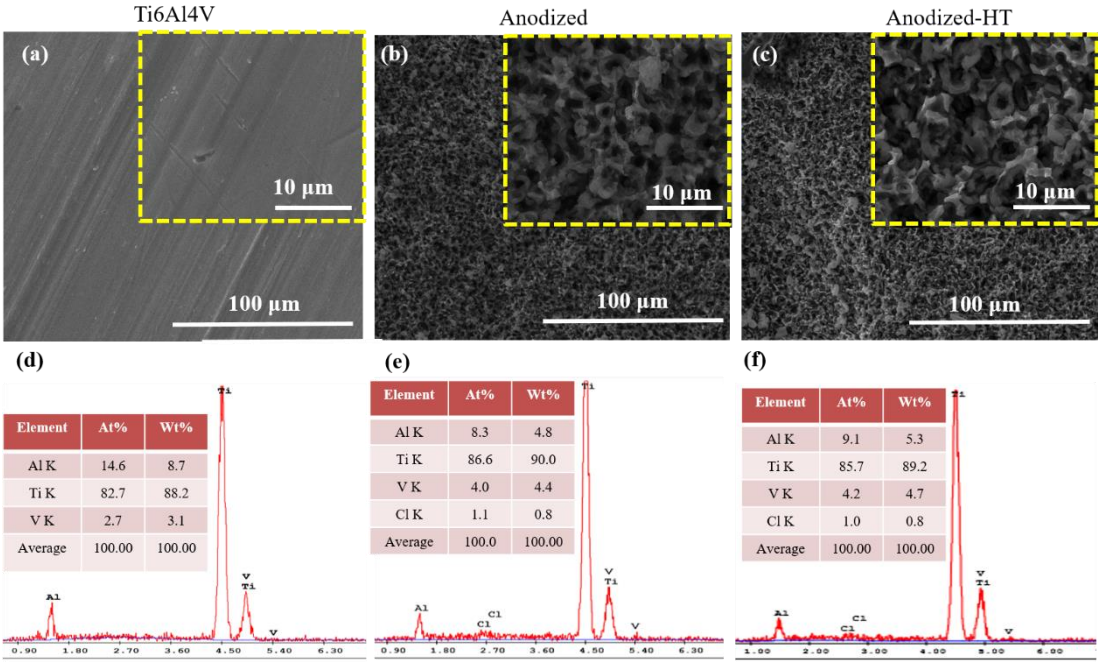
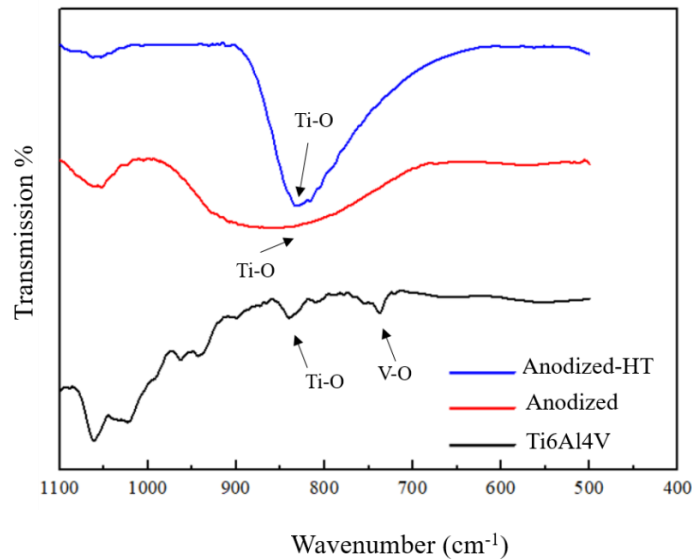


Figure 2.2: (a), (b) and (c) SEM images and (d), (e) and (f) EDS spectra of (a) and (d) Ti6Al4V, (b) and (e) Anodized, (c) and (f) Anodized-HT samples. Insets show higher magnification images of samples.



The influence of anodization and the follow-up heat treatment process on the surface chemical structure of Ti6Al4V samples was investigated by Fourier Transform Infrared (FTIR) spectroscopy and the results were displayed in Fig. 2.3. Stretching vibrations consistent with Ti-O bonding were detected around 850  $\text{cm}^{-1}$  for all samples [82]. It was also observed that Anodized and Anodized-HT surfaces expressed more intense Ti-O bands on their surfaces compared to Ti6Al4V (non-anodized) samples, which could be attributed to the growth of oxide layer during anodization and follow-up heat treatment. In the FTIR spectra of Ti6Al4V, V-O stretching vibrations were detected around 720  $\text{cm}^{-1}$  [83]. In this research, no vanadium or aluminum peaks appeared for anodized and anodized-HT samples, which was in-line with previous researchers [84].



*Figure 2.3: FTIR spectra of Ti6Al4V (black line), Anodized (red line) and Anodized-HT (blue line) samples*

To investigate the crystal structure of the samples, XRD scans were taken and the results were presented in Fig.2.4. The XRD spectra showed characteristic peaks belonging to Ti6Al4V for all samples. Ti- $\alpha$  peaks appeared at 35.4°, 38.5°, 40.5° and 53.3° (JCPDS file #44-1294), which belonged to (100), (002), (101) and (102) planes, respectively, and Ti- $\beta$  peak appeared at 39.5° (JCPDS file #44-1288), which belonged to (110) plane for all investigated samples. XRD characterization did not show any

crystalline phase for the oxide based micropit patterns. It was well-established that anodized oxide layers had amorphous crystal structure, which lacked ordered planes to appear on the XRD spectra [85]. For the case of Anodized-HT samples, the diffraction peaks were ascribed to anatase phase at  $25.37^\circ$  and  $38.67^\circ$  (JCPDS #01-0562), which correlated with (101) and (112) planes, respectively. Based on previous studies, annealing of titanium alloys above  $400^\circ\text{C}$  transformed anodized amorphous surface structures to anatase, while annealing at around  $600^\circ\text{C}$ , transformed anatase to rutile [86]. Formation of crystalline titanium oxide is favored in orthopedics since presence of anatase correlated with greater biocompatibility compared to amorphous titanium oxide [87, 88].

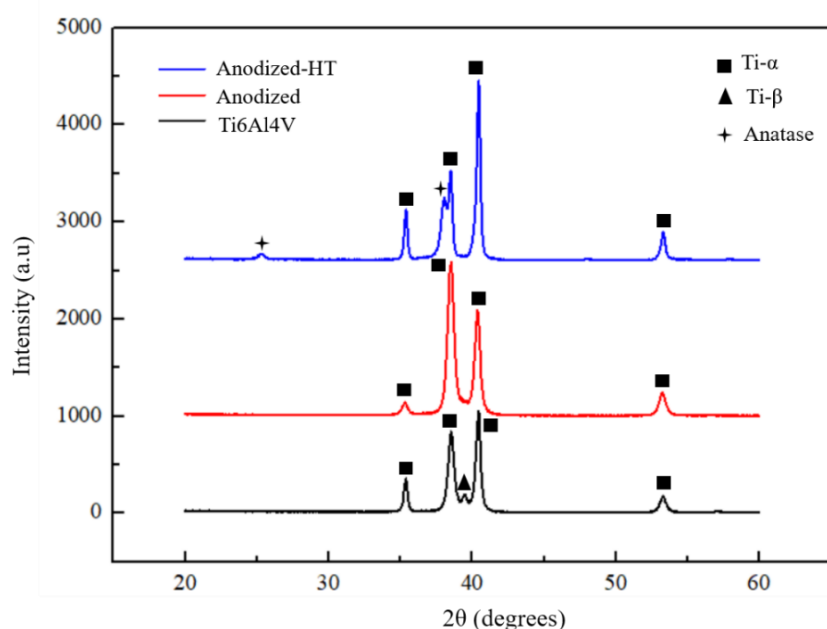


*Figure 2.4: XRD spectra of Ti6Al4V (black line), Anodized (red line) and Anodized-HT (blue line) samples.*

HR-TEM images and electron diffraction patterns of Anodized and Anodized-HT samples were shown in Fig. 2.5a and b, respectively. TEM characterizations confirmed that the anodized oxide layer on Ti6Al4V samples was amorphous and the corresponding SAED pattern was in accord this finding. For the case of Anodized-HT

samples, HR-TEM image and the corresponding SAED pattern confirmed XRD results (Fig. 2.5) and demonstrated anatase phase upon heat treatment at 500°C.

The lattice fringes obtained from the HR-TEM image exhibited a d-spacing of 0.32 nm corresponding to (101) plane of anatase [89]. Thus, these results further confirmed transformation of amorphous oxide layer to anatase after the heat treatment process.

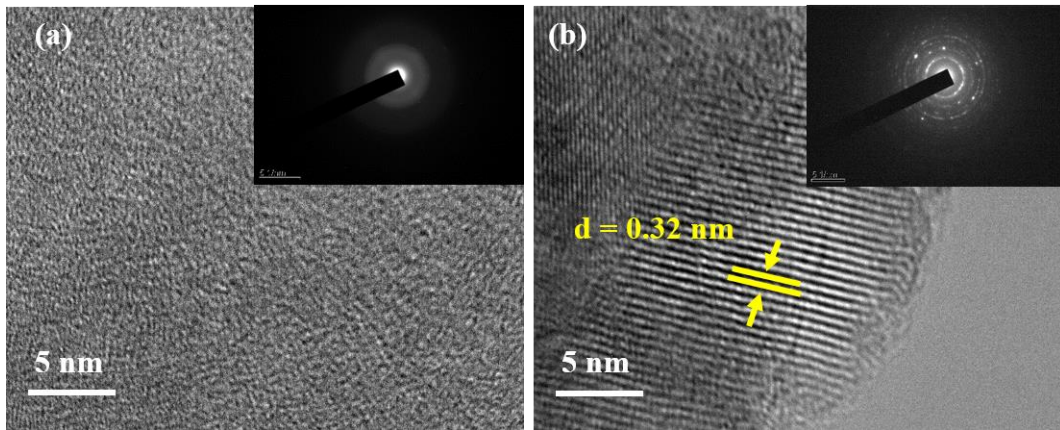


*Figure 2.5: HR-TEM images of (a) Anodized and (b) Anodized-HT samples. Insets show SAED patterns obtained from these samples.*

To investigate surface chemical composition of the samples, XPS depth profiles analysis was completed. As shown in Fig. 2.6, concentration of carbon (indicated with green line) on Ti6Al4V surfaces was the highest and it decreased after anodization and heat treatment procedures. Carbon was a contaminant on Ti6Al4V surfaces and it potentially originated from the organic solvents used to clean specimen surfaces [90]. Since anodization etched the surface in contact with electrolyte during micropit formation, the adsorbed carbon content on all surfaces decreased during anodization. Once anodized Ti6Al4V samples were heat treated, carbon contamination decomposed from the surfaces. Upon sputtering the samples surface, carbon content decreased drastically independent of the sample type, suggesting surface adsorption was the main mechanism for the presence of carbon contamination [91]. As opposed to carbon, oxygen content (indicated with red line) followed an opposite trend where its concentration increased after anodization compared to Ti6Al4V samples. This was expected since the purpose of anodization in this study was to intentionally grow oxide

layer on Ti6Al4V. When surfaces were sputtered, there were no significant changes in the oxygen concentrations since an 8 min sputter was not sufficient to remove micron thick pits from the surfaces. Titanium content of the samples (indicated with black line) were low on all specimen surfaces, yet its concentration increased significantly upon sputtering the top surface, which was probably removal of carbon contamination observed on the surfaces. Ti6Al4V sample had the highest titanium content on its surface, followed by Anodized-HT and Anodized samples. Aluminum and vanadium concentration of Ti6Al4V surface followed a similar trend where they were highest on Ti6Al4V samples, followed by Anodized and Anodized-HT samples. Cumulatively speaking, the surface compositions of Ti6Al4V, Anodized and Anodized-HT samples were different from each other and these differences would certainly influence biological properties of the samples and alter their bioactivity.

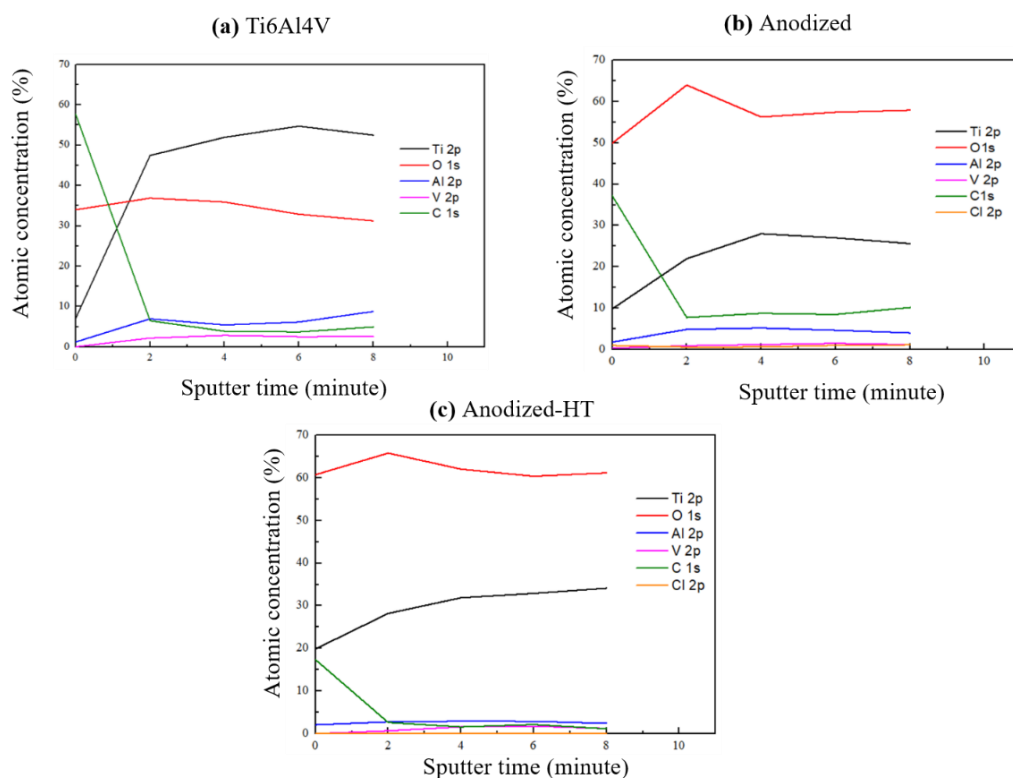
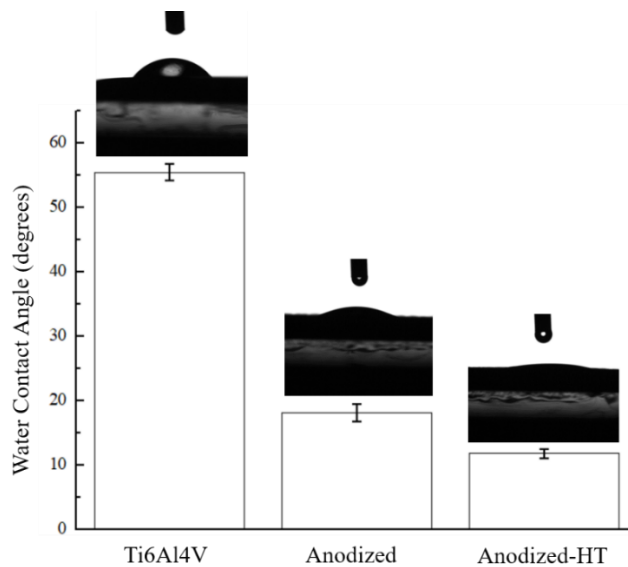


Figure 2.6: XPS depth profiles of (a) Ti6Al4V, (b) Anodized and (c) Anodized-HT samples. Samples were sputtered with Ar<sup>+</sup> five times each for two minutes.

To investigate the wettability of samples, water contact angles for Ti6Al4V, Anodized and Anodized-HT were measured and reported in Fig.2.7. It was observed that water contact angles for Anodized and Anodized-HT samples were significantly lower than Ti6Al4V samples, indicating hydrophilic nature of these surfaces. As a matter of fact, water contact angle for Anodized-HT reached as low as 12°. The increase in hydrophilicity of anodized surfaces could be explained with changes in chemical composition and topography of the Anodized and Anodized-HT sample surfaces compared to Ti6Al4V. It should be noted that increase in hydrophilicity of orthopedic implants was typically associated with enhanced bioactivity of orthopedic implants [92].



*Figure 2.7: Sessile drop water contact angles of Ti6Al4V, Anodized and Anodized-HT samples. Values are reported as mean ± EM; N=5 and n=4.*

In order to assess delamination resistance of the anodized micropit surfaces, microscratch tests were completed using a 5 µm radius Berkovich tip indenter. In Fig.2. 8a, the penetration depth at delamination was observed to be approximately 15 µm (See Fig. S8) at a scratch distance of 0.3 mm. Within this scratch distance, friction force of samples increased to 0.7 N, which corresponded to the delamination of coatings from the Ti6Al4V substrate. In the literature, Souza *et al.* anodized titanium in a mixture of (CH<sub>3</sub>COO)<sub>2</sub>.Ca.H<sub>2</sub>O and NaH<sub>2</sub>PO<sub>4</sub>.2H<sub>2</sub>O (fluoride-free) solution to

obtain a rough and porous surface [93]. Scratch tests on these surfaces reported 220 mN of applied load for the anodic layer to delaminate. In addition to this, Smith *et al.* reported fabrication of anodized nanotubular titanium oxide surface using a mixture of diethylene glycol with 2% HF under 60V for 24 hours [94]. When these surfaces were examined under scratch tests, the critical load was found to be approximately 0.33N. In literature, the use of fluorinated electrolytes during anodization proposed to be one of the reason for the weak adhesion of titanium oxide layer onto the substrate metal, where electrical field induced migration and accumulation of fluoride ions at the bottom of nanotubular films was the reason behind weak cohesion [95]. Since fluoride ions did not exist in the electrolyte in the designed anodization process, fluoride ions could not accumulation within the oxide film, and thus stronger cohesion of the oxide layer onto the Ti6Al4V substrate was obtained. Though more research is required on the mechanism of oxide film delamination from the underlying substrate, to the best of our knowledge, this was the first published data quantifying the delamination force of oxide layer grown using a chloride based electrolyte onto its Ti6Al4V substrate.

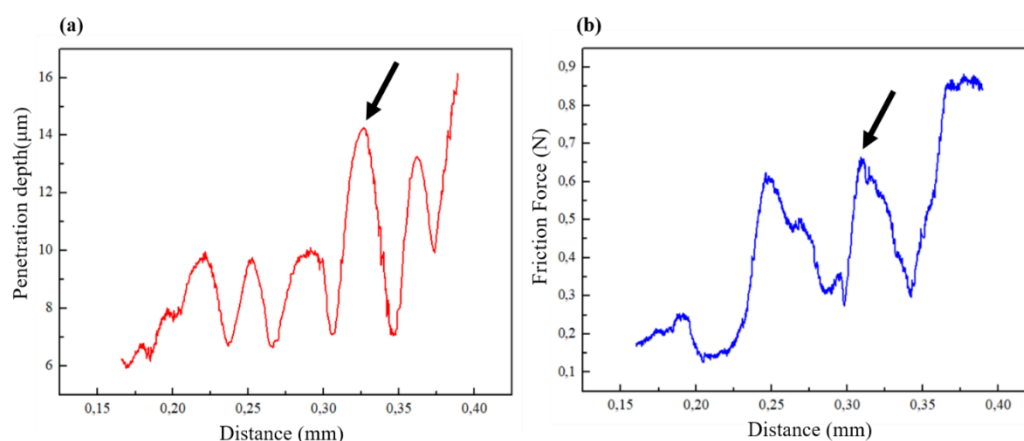


*Figure 2.8: Microscratch test results showing (a) penetration depth vs. distance and (b) friction force vs. distance for Anodized samples.*

Fig.2.9 shows SEM images of the samples after a 30 day exposure to SBF. By comparing Fig. 2 and Fig. 9, it could be observed that surface morphology of Anodized and Anodized-HT samples changed upon interacting them in SBF for 30 days, however no visible change was observed for Ti6Al4V samples. EDS spectra detected the presence of Ca and P elements on all samples, while concentrations of these

elements were much higher on Anodized and Anodized-HT samples compared to Ti6Al4V. The bioinert nature of Ti6Al4V could be attributed to the lack of significant CaP mineral formation on these surfaces. Upon anodization, hydrophilicity of the samples increased, along with changes in surface chemical composition. Since both of these parameters influence bioactivity of materials, increased CaP mineral formation was observed on Anodized samples compared to Ti6Al4V. For the case of Anodized-HT, sample surface transformed to crystalline anatase phase. In the literature, crystalline titanium oxide (both anatase and rutile) was documented to enhance bioactivity, and thus it plausible to claim that heat treatment process also contributed to the formation of CaP crystals [84].

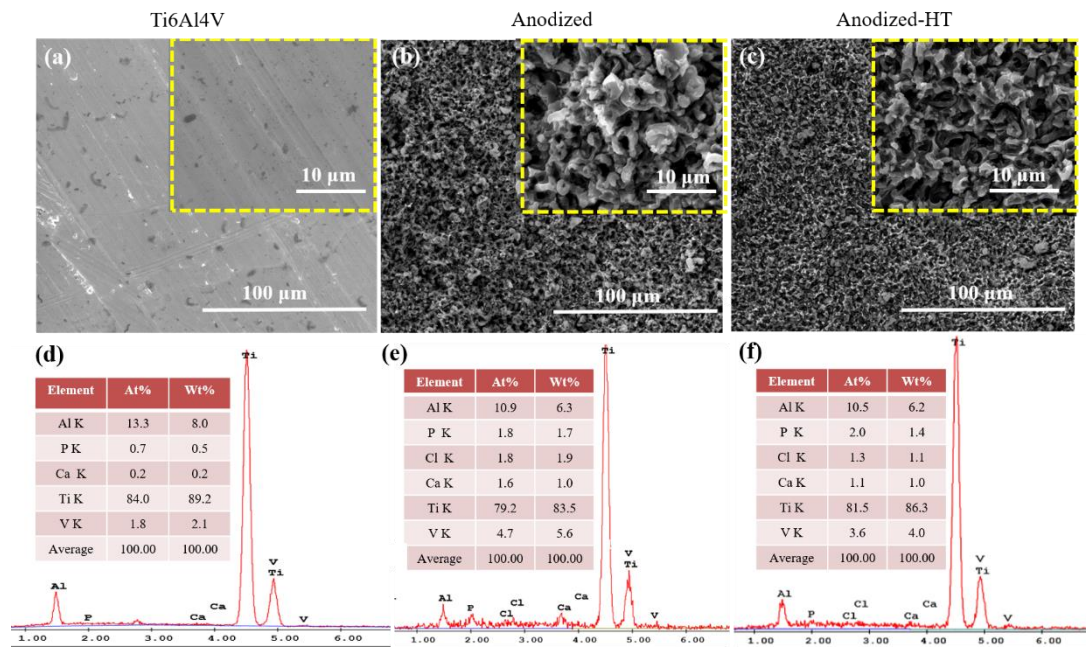
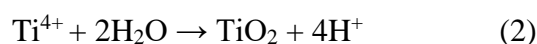


Figure 2.9: (a), (b) and (c) SEM images and (d), (e) and (f) EDS spectra of (a) and (d) Ti6Al4V, (b) and (e) Anodized, (c) and (f) Anodized-HT samples immersed in 1x SBF for 30 days. Insets show higher magnification images of samples.

Although the mechanism of anodization using chlorinated electrolytes has not been fully understood, it was reported that micropits appeared on titanium surfaces via rapid breakdown anodization, which was the local breakdown of oxide film by chloride ions and formation of irregular patterns on the surface [95-97]. In fact, the growth of micropits depended on the formation of an oxide film at the metal/oxide interface and

electrochemical dissolution of this oxide film at the oxide/electrolyte interface. Briefly, small pits with different shapes and sizes randomly nucleate on Ti6Al4V surfaces. When voltage is applied to Ti6Al4V anode, an oxidation reaction starts at the metal/metal oxide interface on Eq. (1) and produce  $Ti^{4+}$  ions. These  $Ti^{4+}$  ions migrate outwards under the applied voltage, while  $O^{2-}$  ions present in the electrolyte migrated towards the metal/metal oxide interface. During migration of negatively charged  $O^{2-}$  ions, they encounter  $Ti^{4+}$  ions ejected from the surface and react to generate a compact oxide film shown Eq. (2). The growth of passive oxide layer on Ti6Al4V substrate leads to an increase in resistance and reaction speed decreases. Once micropits form, reaction of titanium oxide film with  $NH_4Cl$  takes place on Eq. (3). These reactions simultaneously occur during anodization and they are summarized below:



Anodized and anodized-HT samples fabricated using the optimized parameters (0.4 M  $NH_4Cl$  electrolyte under 30V potential for 2 min.) had desired properties for orthopedic applications. Specifically, Anodized and Anodized-HT samples had a higher surface roughness, increased surface area and hydrophilicity compared to non-anodized Ti6Al4V samples. Upon heat treatment of anodized samples, amorphous titanium oxide transformed into anatase phase, which has been documented to enhance bone cell functions and mineralization *in vitro* [98]. These changes favored bioactivity and led to increased mineralization of the Anodized and Anodized-HT samples in this research. Additionally, aforementioned changes in the surface properties of an implant also influences adsorption of proteins onto the implant surfaces, which further controls initial adhesion of bone cells onto the orthopedic implant surfaces. As a matter of fact, anodized titanium surfaces were shown to promote adsorption of higher concentrations of vitronectin and fibronectin proteins from serum, which acted as anchorage points for attachment of bone cells via their integrin surface proteins [99]. Enhanced adhesion of bone cells and upregulated cellular functions were correlated with improve



osseointegration with the juxtaposed tissue and these observations were confirmed *in vitro* and *in vivo* by different researcher groups [100]. *In vitro* experiments showed enhanced adhesion, proliferation, cellular functions (*i.e.* alkaline phosphatase activity, collagen type I and calcium synthesis) and up-regulation of osteogenic genes on anodized Ti6Al4V surfaces compared to conventionally-used Ti6Al4V [49]. When osseointegration of machined, grit blasted and anodized Ti6Al4V implants were tested, pull-out tests presented stronger integration of the anodized Ti6Al4V implants compared to machined and blasted ones after four week implantation into the femoral condyles of rabbits [101]. Histology examinations revealed direct apposition of bone tissue with higher bone to implant contact area for anodized Ti6Al4V implants compared to machined and grit blasted surfaces. Puckett *et al.* examined anodized Ti6Al4V pins using a unilateral through the knee rat amputation model. It was reported that animals implanted with anodized Ti6Al4V pins walked much earlier and anodized pins supported an increase in bone-to-implant contact compared to conventional Ti6Al4V pins [102].

Although aforementioned studies confirmed potential improvements in bone cell functions upon anodization and this research provided evidence for improved CaP mineral formation on Anodized and Anodized-HT samples, it is still not clear if fabricated surfaces will improve biological response. This research obtained preliminary results for anodization of Ti6Al4V to fabricate surface micropits and showed its potential for enhancing bioactivity. Though further research is required to investigate *in vitro* bone cell functions, micropit surfaces have the potential to improve osseointegration and deserves further investigation.

### 2.3. Supporting Information: Fabrication of Micropit Structures Using Fluoride Free Anodization

In this part, supporting information is presented.

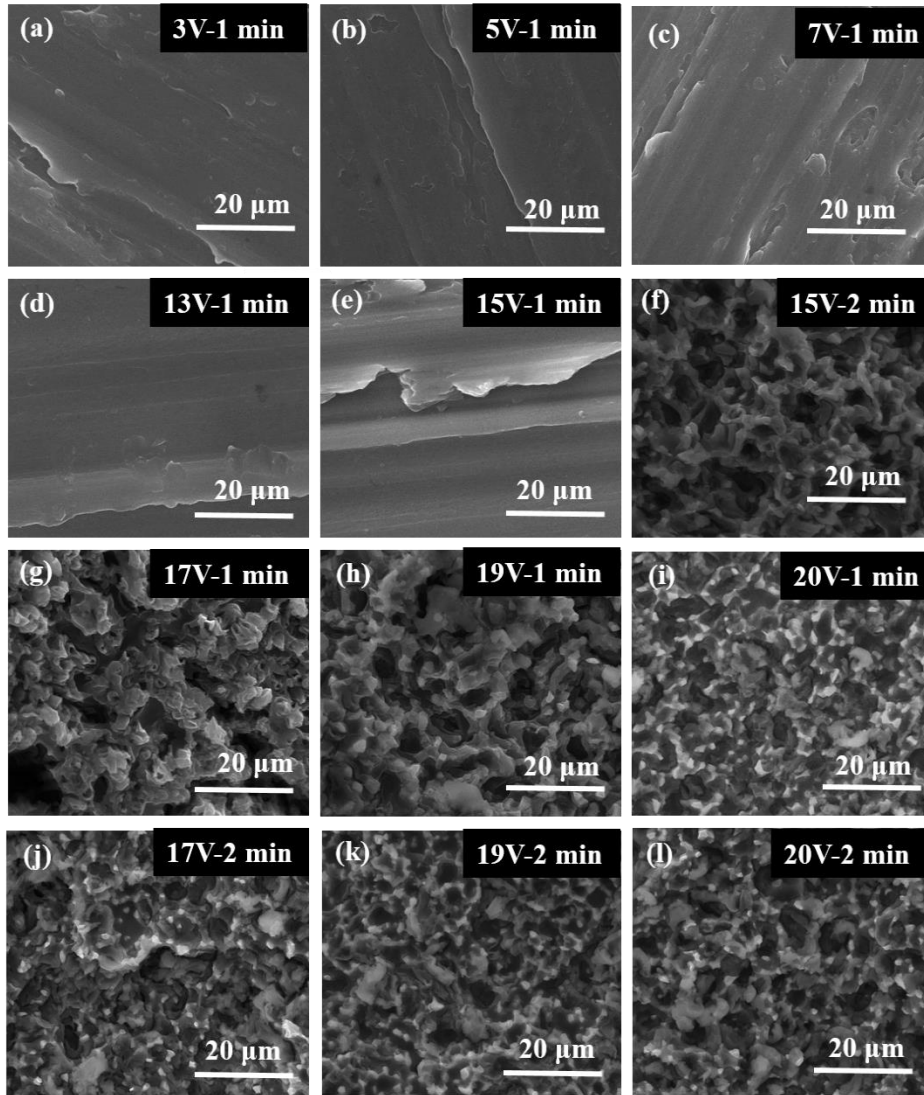


*Figure S1: SEM images of Ti6Al4V samples anodized using 0.3 M NaCl electrolyte. Anodization was conducted under (a) 3V for 1 min, (b) 5V for 1 min, (c) 7V for 1 min, (d) 13V for 1 min, (e) 15V for 1 min, (f) 15V for 2 min, (g) 17V for 1 min, (h) 19V for 1 min, (i) 20V for 1 min, (j) 17V for 2 min, (k) 19V for 2 min and (l) 20V for 2 min.*

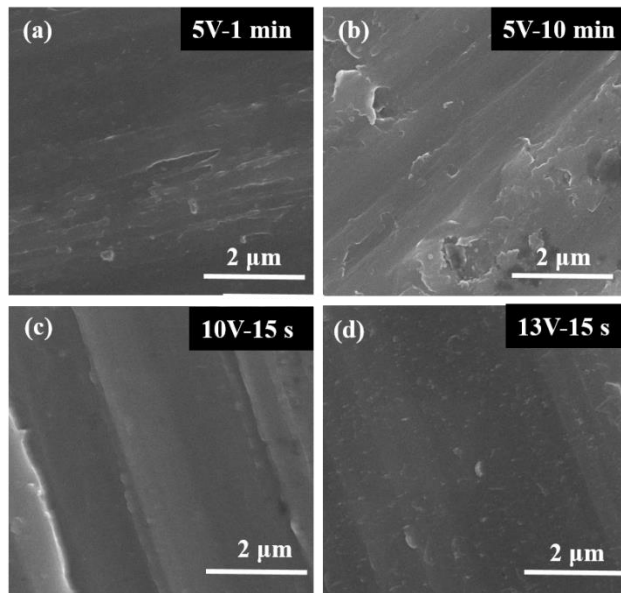


*Figure S2: SEM images of Ti6Al4V samples anodized using 3M HCl electrolyte. Anodization was conducted under (a) 5V for 1 min, (b) 5V for 10 min, (c) 10V for 15sec and (d) 13V for 15 sec. Anodization using 3M HCl did not form any surface structures Ti6Al4V samples under the investigated conditions*

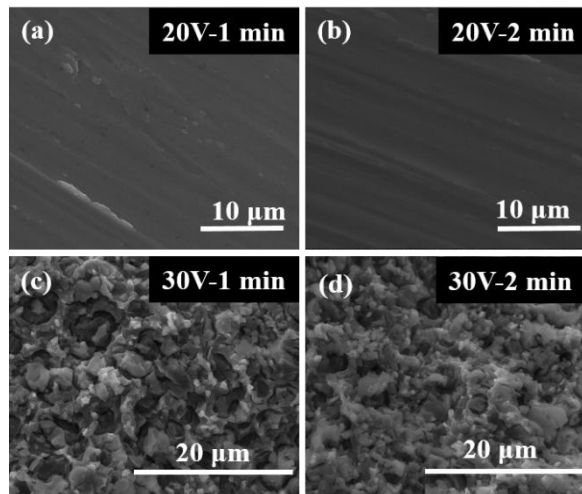


*Figure S3: SEM images of Ti6Al4V samples anodized using 0.02 M HCl electrolyte. Anodization was conducted under (a) 20V for 1 min, (b) 20V for 2 min, (c) 30V for 1 min and (d) 30V for 2min.*

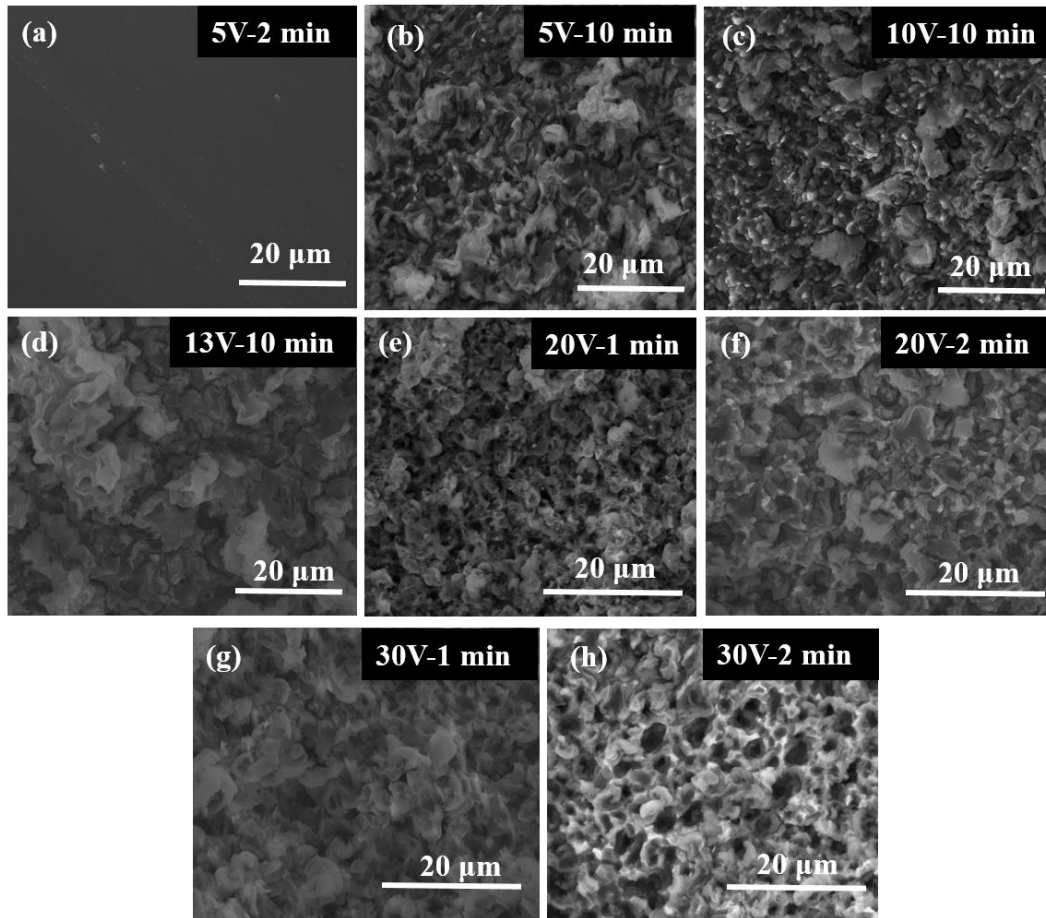


*Figure S4: SEM images of Ti6Al4V samples anodized using 0.02 M HCl and 0.4 M NH<sub>4</sub>Cl electrolyte. Anodization was conducted under (a) 5V for 2 min, (b) 5V for 10 min, (c) 10V for 10min, (d) 13V for 10min, (e) 20V for 1 min (f) 20V for 2 min, (g) 30V for 1min and (h) 30V for 2 min*

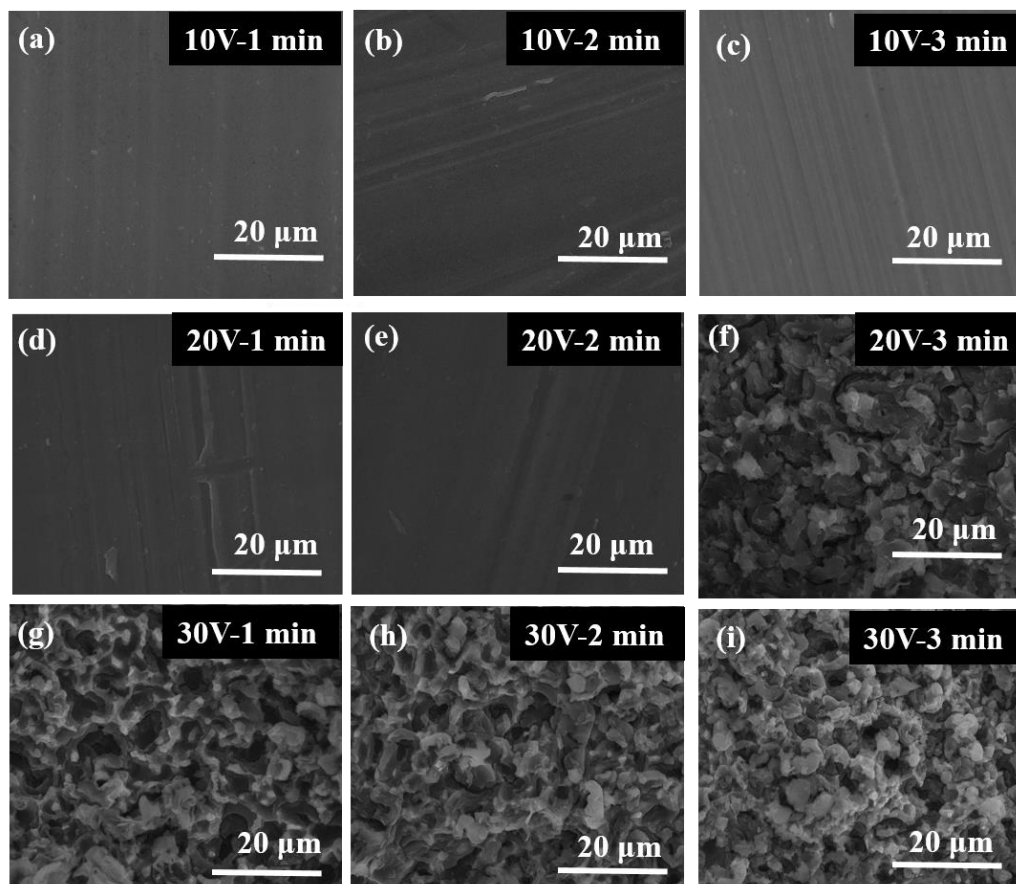


*Figure S5: SEM images of Ti6Al4V samples anodized using 0.2M NH<sub>4</sub>Cl electrolyte. Anodization was conducted under (a) 10V for 1 min, (b) 10V for 2 min, (c) 10V for 3min, (d) 20V for 1min, (e) 20V for 2 min, (f) 20V for 3 min, (g) 30V for 1 min, (h) 30V for 2 min and (i) 30V for 3min.*

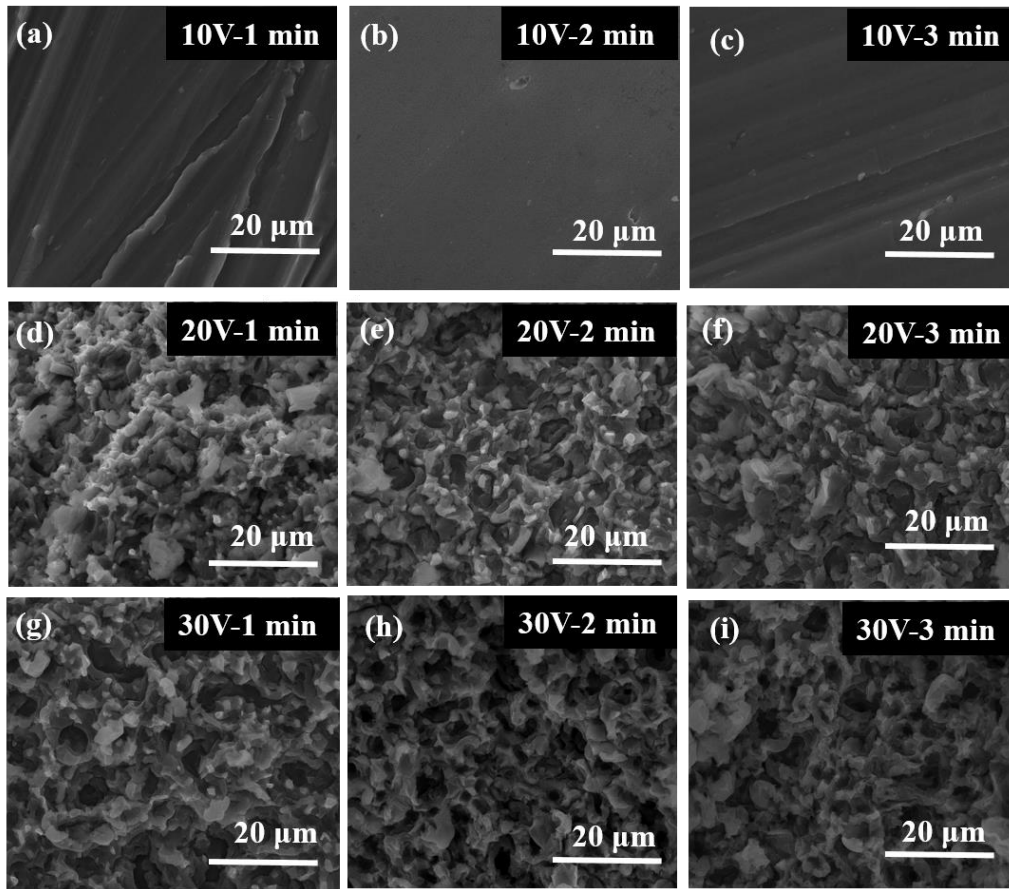


*Figure S6: SEM images of Ti6Al4V samples anodized using 0.4M NH<sub>4</sub>Cl electrolyte. Anodization was conducted under (a) 10V for 1 min, (b) 10V for 2 min, (c) 10V for 3min, (d) 20V for 1min, (e) 20V for 2 min, (f) 20V for 3 min, (g) 30V for 1 min, (h) 30V for 2 min and (i) 30V for 3min.*

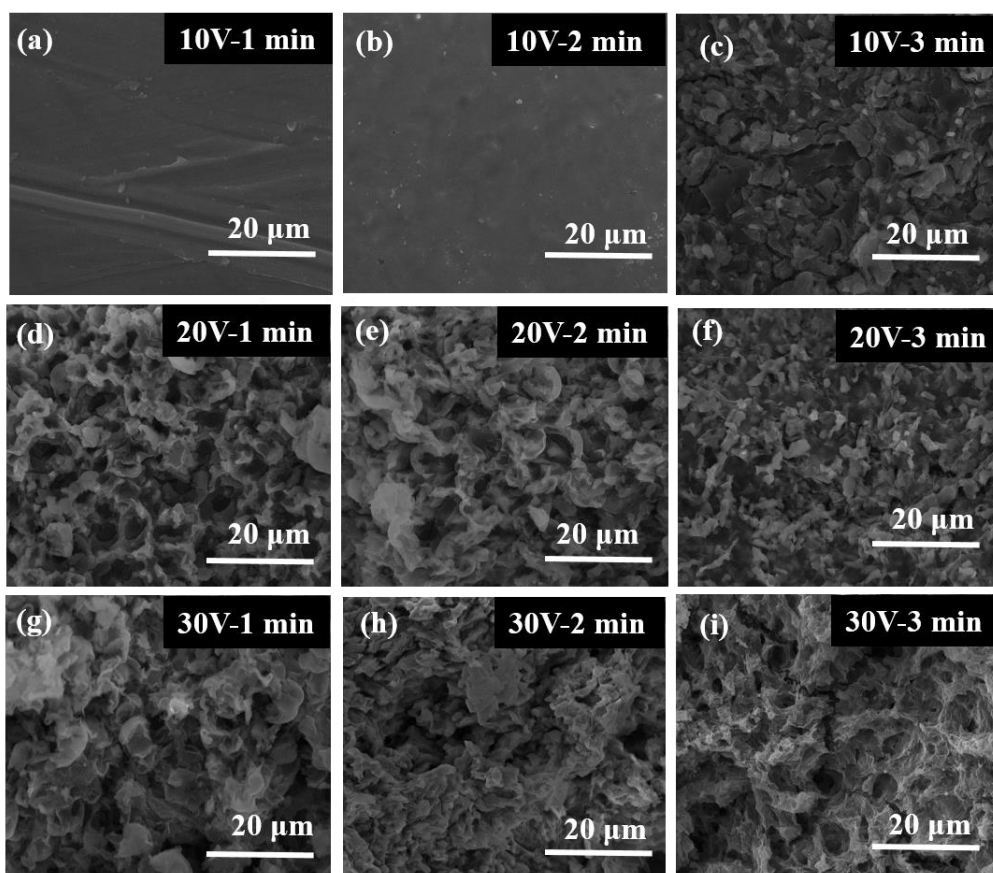


*Figure S7: SEM images of Ti6Al4V samples anodized using 0.6M NH<sub>4</sub>Cl electrolyte. Anodization was conducted under (a) 10V for 1 min, (b) 10V for 2 min, (c) 10V for 3min, (d) 20V for 1min, (e) 20V for 2 min, (f) 20V for 3 min, (g) 30V for 1 min, (h) 30V for 2 min and (i) 30V for 3min.*

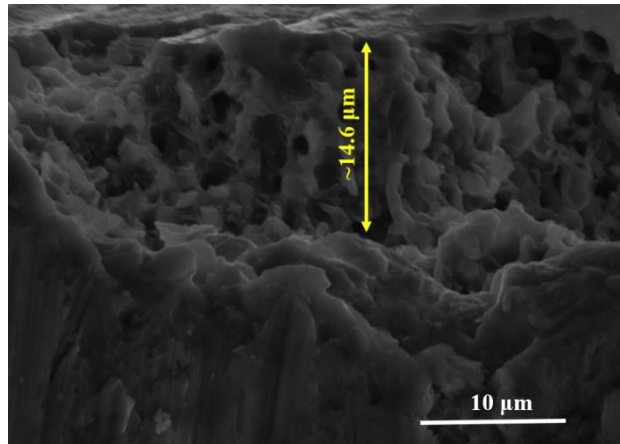


Figure S8: SEM cross sectional image of Anodized samples showing the approximate oxide layer thickness.

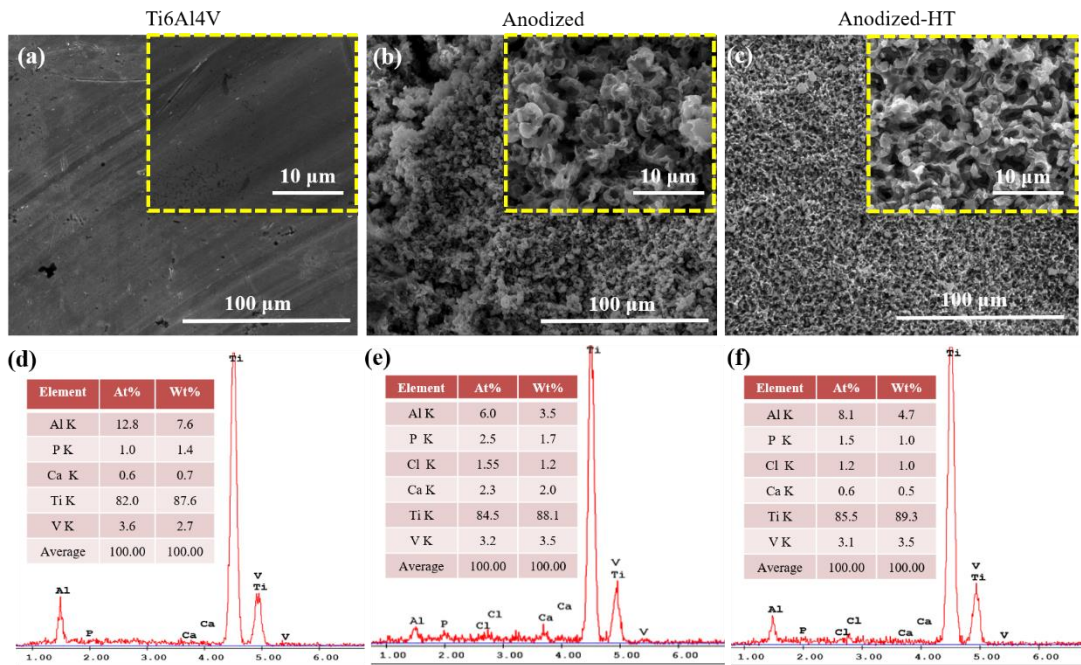


Figure S9: (a), (b) and (c) SEM images and (d), (e) and (f) EDS spectra of (a) and (d) Ti6Al4V, (b) and (e) Anodized, (c) and (f) Anodized-HT samples immersed in 1x SBF for 15 days. Insets show higher magnification images of samples.



## **CHAPTER 3**

### **INTERACTION OF ANODIZED Ti6Al7Nb WITH SIMULATED BODY FLUID**

The present work investigates modification of Ti6Al7Nb alloy surfaces using anodization for orthopedic applications. By optimizing the anodization parameters, nanotubular oxide layers with tubular diameters tailored between 25 nm to 140 nm was fabricated on Ti6Al7Nb alloy surfaces. When Ti6Al7Nb samples possessing nanotubular surface features were immersed in simulated body fluid for 30 days, calcium phosphate mineral formation was observed on these surfaces. Results showed that anodized Ti6Al7Nb samples with 140 nm diameter had a higher bioactivity compared to samples with 25 nm nanotubular diameter and non-anodized Ti6Al7Nb samples, and thus anodized Ti6Al7Nb is a promising candidate for orthopedic applications.

### **3.1. Experimental Details**

#### **3.1.1. Sample preparation**

An 18 mm diameter Ti6Al7Nb rod (ASTM F1295 ISO 5832-11) was cut to a thickness of 1 mm using a precision cutter (Buehler, Linear Precision Saw). The cut pieces were cleaned with sonication using acetone, ethanol (96% Pur. Gr.) and ultrapure water, respectively, for 20 minutes each. The cleaned Ti6Al7Nb specimens were anodized using the apparatus shown in Fig. 2.1. During anodization, the platinum mesh was used as the cathode and the cleaned Ti6Al7Nb specimens were used as the anode. The platinum mesh and Ti6Al7Nb specimens used were connected to a direct current (DC) power supply (TDK-Lambda Genesys 300V / 5A) via copper wire, and a mixture of 1.4M H<sub>3</sub>PO<sub>4</sub> and 0.0115M HF was used as the electrolyte solution. During the anodization process, the electrolyte solution was magnetically mixed, and the applied voltage was altered from 5V and 30V. Once electrochemical process was complete, the anodized specimens were washed with ultrapure water and dried at room temperature and heat-treated at 600 °C for 1 hour. In this work, the heat-treated specimens were denoted by HT. Anode. 25, Anod. 50, Anod. 80 and Anod. 140 refers to 25 nm, 50 nm, 80 nm and 140 nm diameter nanotubular structures, respectively.

#### **3.1.2. Preparation of simulated body fluid**

As mentioned above the section 2.1.2, simulated body fluid was prepared and then Ti6Al7Nb samples with different nanotubular structures were immersed in them up to 30 days.

#### **3.1.3. Surface Characterizations**

Specimens were characterized using scanning electron microscopy (FESEM FEI NOVA NANO 430) to confirm the formation of nanotubular oxide structure on Ti6Al7Nb alloy surfaces and to image the resulting surface morphology. In the SEM studies, 20 kV accelerating voltage was used to display the surfaces. To investigate inner and outer surface morphologies and lengths of nanotubular surfaces grown on

Ti6Al7Nb specimens, transmission electron microscope (TEM, JEOL JEM 2100F) was used. During these studies, a 200-kV accelerating voltage and 14.20 convergence angles was used. Surface chemical analyzes were performed using energy dispersive spectrometry (EDAX-AMETEK) and Fourier Transform Infrared Spectroscopy (FTIR, Perkin Elmer 400) to determine the functional groups and molecular structures on the surfaces. For FTIR, The surface was scanned at mid-IR ( $4000\text{-}500\text{ cm}^{-1}$ ) and the  $\text{OH}^-$ ,  $\text{PO}_4^{3-}$ , and  $\text{CO}_3^{2-}$  bands on the surfaces were characterized. Statistical comparisons in these studies were performed using Student's t-test. All experiments were repeated 3 times, the diameters of nanotubular structures were calculated from 20 different regions and the FTIR analyses were repeated 16 times.

### **3.2. Results and Discussion**

When anodized Ti6Al7Nb specimens were examined, it was determined that nanotubular structures were obtained on the surfaces of the specimens. It was shown that the diameter of nanotubular structures formed can be changed in a controlled manner from 25 nm to 140 nm by changing the potential applied during the anodization (Figure 3.1). Prior to the anodization, Ti6Al7Nb-HT specimens are shown in Figure 3.1a. When anodization was carried out by applying 5V to Ti6Al7Nb specimens, tubular structures began to form on the surface of the specimens (Fig. 3.1b). A significant increase in the diameters of the tubular structures occurred when the voltage was increased to 10V, 20V, and 30V (Fig.3. 1c, 1d, and 1e).

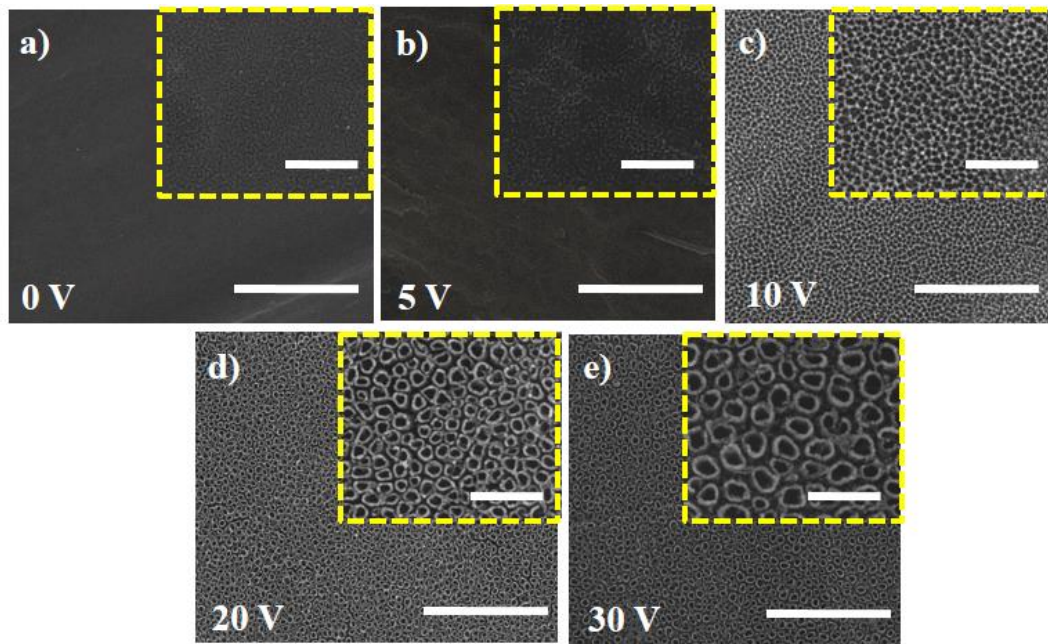


*Figure 3.1: SEM images of a) Ti6Al7Nb-HT, b) Anod. 25-HT, c) Anod. 50-HT, d) Anod. 80-HT ve e) Anod. 140-HT samples. Scale bars are  $3\mu\text{m}$  for lower magnification images and  $500\text{ nm}$  for higher magnification images.*

Findings obtained after the anodization were similar to the literature. As observed in different titanium alloys, it was determined that the controlled deformation of the nanotubular structures formed on the anodized surface was depending on the potential applied during anodization [103]. In this study, it was observed that the diameters of nanotubular structures increase with increasing applied voltage (Figure 3.2). However; it was determined that this increase was also an upper limit, and current electrolyte and electrochemical parameters applied to the Ti6Al7Nb specimens at the voltages at 35V and above caused cracks in the tubular structures where the nanotubular structures were deteriorating and the tubular morphology began to disappear (this data cannot be shown as the nanotubular morphology began to disappear).

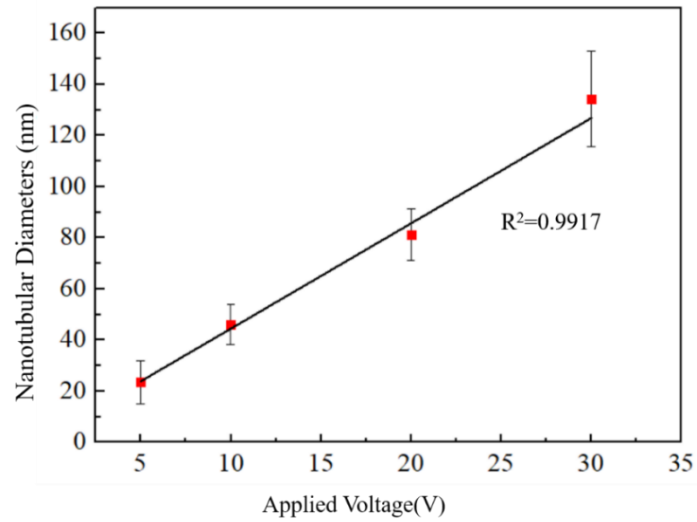


Figure 3.2: Change of nanotubular diameters on Ti6Al7Nb samples with applied voltage. Values are reported as mean  $\pm$  SEM;  $N=20$ ,  $n=3$ .

In the characterization studies carried out by TEM, it was confirmed that the nanotubular structures were formed on the surfaces obtained by the anodization. In Fig. 3.3, it is shown that the nanotubular structures produced by applying 20V are 80 nm in diameter and 280-350 nm in length. The length ratios of the obtained structures varied between approximately 3.5 and 4.5, and this ratio first increased in the formation phase of the nanotubes (tube formation phase), and as the anodization time progressed, the length ratios of the nanotubular structures decreased due to the disappearance of the nanotubular structures over time in the acid environment. If the chemical dissolution of the HF-containing electrolyte solutions is faster than the formation of the oxide layer, the length of the nanotubular structures for anodized titanium metal, which is determined Oh *et al.*, is reduced [104]. However, it was observed that the length ratios of the nanotubular structures obtained at different voltages were different (provided all other anodization parameters were kept constant).

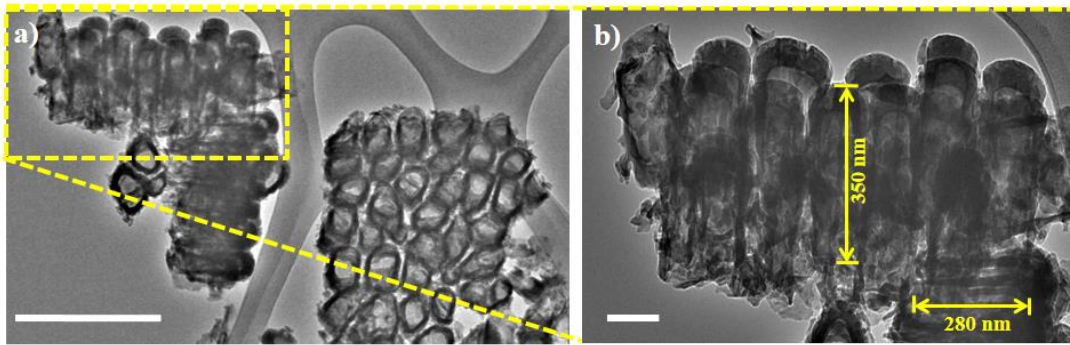
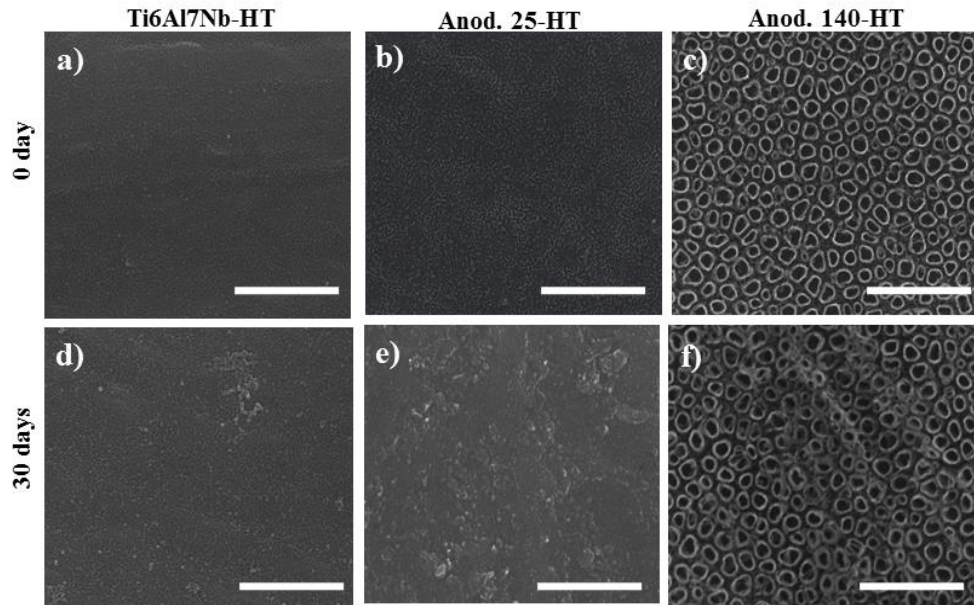


Figure 3.3: a) Lower and b) higher magnification TEM images of the oxide layer formed on Ti6Al7Nb anodized at 20 V. Scale bars are a) 500 nm and b) 100 nm.

Our research group is deeply studying the formation kinetics of nanotubular structures. The fact that the driving force required for the growth of nanotubular structures was the voltage suggests that the change in voltage (which also changes the diameters) brought about a change in length rates. The bioactivities of nanotubular Ti6Al7Nb alloys produced in different diameters were studied in the simulated body fluid for 30 days. It was determined that there are differences between the surfaces of Ti6Al7Nb-HT that was soaked in simulated fluid in SEM characterizations, Anod. 25-HT and Anod. 140-HT. It was also determined that surface morphology was preserved while calcium phosphate formation occurred on the surfaces of the Ti6Al7Nb-HT (Figs. 3.4a and 3.5d) and Anod. 140-HT (Fig. 3.4b and 4e) resulting from the simulated body fluid of the nanotubular structures formed in the Anod. 25-HT (Fig. 3.4b and 4e) specimen. In the specimens of 140-HT (Figs. 5c and 5f), it was determined that surface morphology was preserved while calcium phosphate formation occurred on the surfaces



*Figure 3.4: SEM images of Ti6Al7Nb alloys a), b) and c) before and d), e) and f) after 30-days exposure to simulated body fluid. Samples are a) and d) Ti6Al7Nb-HT, b) and e) Anod. 25-HT and c) and f) Anod. 140-HT. Scale bars are 1 $\mu$ m.*

Ti6Al7Nb-HT was thought to be in relation to the bioactive of titanium alloys that were not at the desired level due to the low calcium phosphate precipitated on the specimen surface. The fact that the 140 nm diameter nanotubular surfaces were not completely covered is due to the fact that the precipitated calcium phosphate crystals were smaller in size than the nanotubular structures and couldn't completely cover the surfaces of the tubular structures (some calcium phosphate precipitates into the tubular structures); on the contrary, On the contrary, it can be speculated that the nanofeatures on 25nm diameter surface did not appear because the dimensions of calcium phosphate precipitated on specimens were sufficient to completely cover the lower tubular surface. Figure 3.5 showed EDS results after 30 days of interaction with simulated body fluid of Ti6Al7Nb alloys. Calcium and phosphate peaks were found in the EDS spectra taken from each of the Anod. 140-HT Ti6Al7Nb, Ti6Al7Nb-HT, Anod. 25-HT alloys. The presence of these peaks confirmed that all three specimens allowed precipitation of calcium phosphate-based structures from the simulated body fluid (Figs. 3.5a-c).

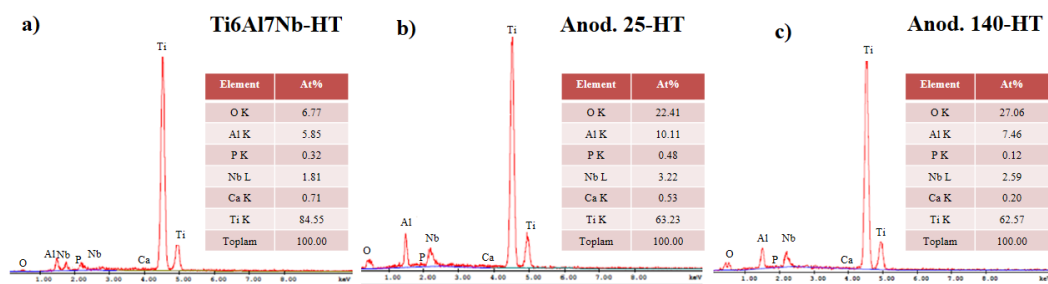


Figure 3.5:EDS spectra of a) Ti6Al7Nb-HT, b) Anod. 25-HT and c) Anod. 140-HT samples after 30 days exposure to SBF.

In Figure 3.7, Ti6Al7Nb-HT, Anod. 25-HT and Anod. 140-HT specimensof FTIR results were given. As a result of the FTIR measurements, it was determined that the peak in the band 813.03 cm<sup>-1</sup> corresponded to the Ti-O-Ti bond in the Ti6Al7Nb-HT specimen and the peak in the band 1198.42 cm<sup>-1</sup> belonged to the P-O bond [105]. In Anod. 25-HT specimen, the peaks at the 667.40 and 817.75 cm<sup>-1</sup> bands corresponded to the Ti-O-Ti bonds [106]. The peaks at 1593.85 and 1281.44 cm<sup>-1</sup> bands on the Anod. 25-HT specimen, and the peaks at 1465.07 and 1367 cm<sup>-1</sup> bands on the Anod. 140-HT specimen were also found to belong to the carbonate (CO<sub>3</sub><sup>2-</sup>) group [107]. In addition, in Anod.140-HT specimen, the peaks corresponding to the P-O bond, which were specific to the phosphate (PO<sub>4</sub><sup>3-</sup>) group in the 140-HT specimen, appeared at 1160,33 and 584,81 cm<sup>-1</sup> [108]. On the Anod. 140-HT specimen, the peak of the OH<sup>-</sup> group, which appeared in the band 1743.27 cm<sup>-1</sup> indicates the adsorbed water [1108], and the Ti-O-Ti bond peak's disappearance on the Anod. 140-HT specimen and (PO<sub>4</sub><sup>3-</sup>) and (CO<sub>3</sub><sup>2-</sup>) peaks' being more prominent indicate that there were more calcium and phosphate mineralization on the Anod.140-HT's surface than 25-HT and Ti6Al7Nb-HT specimens.



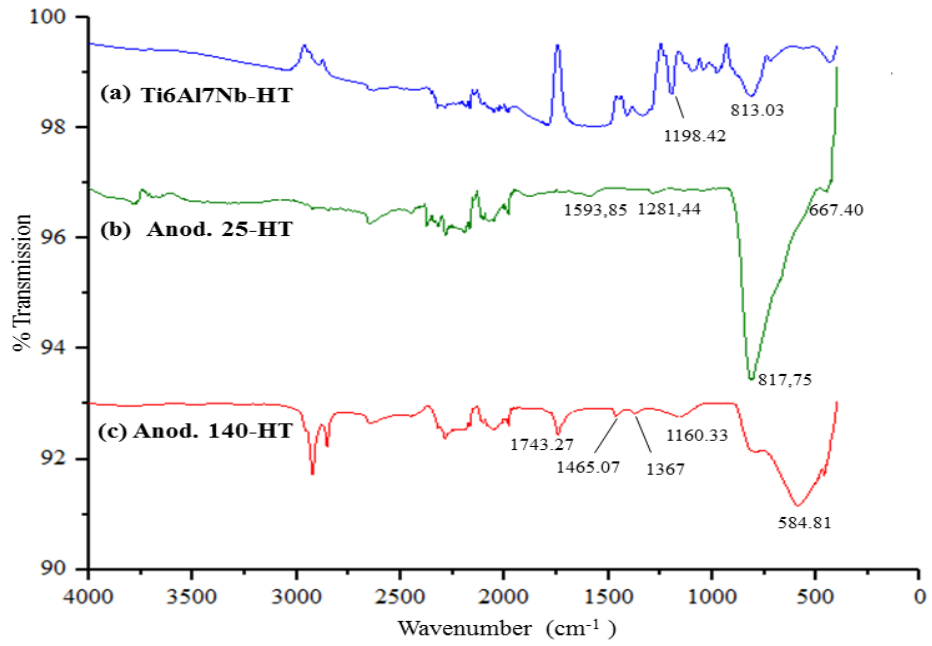


Figure 3.6: FTIR spectra of Ti6Al7Nb surfaces after 30-day interaction with simulated body fluid. Samples are a) Ti6Al7Nb-HT, b) Anod. 25-HT and c) Anod. 140-HT.



## CHAPTER 4

### CONCLUSION AND FUTURE WORK

In this research, fabrication of micropit structures on Ti6Al4V surfaces were investigated, followed by soaking them in simulated body fluid for 30 days. In addition to this, the growth of nanotubular structures with several diameters were studied and then their bioactivities were examined by soaking in simulated body fluid up to 30 days. Within the scope of this research, fabrication and characterization experiments of pit like morphologies and nanotubular structures were carried out and reported.

The conclusions drawn from the results of this research are summarized below:

1. Comprehensive analyses of the fabricated micropit structures and their bioactivities were examined. The results of this research suggest that anodized Ti6Al4V and anodized-HT samples having micropit structures fabricated using a fluoride-free electrolyte can be an effective method to provide bioactive features on Ti6Al4V alloys, and thus potentially enhance the lifetime of Ti6Al4V based orthopedic implants.
2. The interaction between the simulated body fluid with anodized nanofeatured Ti6Al7Nb alloys having different diameters was investigated. Nanotubular structures with 25, 50, 80 and 140 nm diameters were obtained by anodizing in 1.4M H<sub>3</sub>PO<sub>4</sub> + 0.0115M HF electrolyte solution for 1 minute with an applied voltage up to 30 V. The nanotubular structures were heat-treated at 600° C for 1 hour and kept in the simulated body fluid for 30 days. By SEM and EDS analysis, calcium phosphate precipitated on the nanotubular structures was characterized, and phosphates (PO<sub>4</sub><sup>3-</sup>) and

carbonate ( $\text{CO}_3^{2-}$ ) groups on the surface were confirmed by FTIR. The obtained results showed that bioactivity of anodized Ti6Al7Nb specimens of 140 nm diameter increased compared to anodized specimens of 25 nm diameter and non-anodized Ti6Al7Nb specimens. This study confirmed that anodized Ti6Al7Nb having nanotubular surface morphology is a promising material for orthopedic applications.

Apart from these major findings obtained in this research, below points should be considered as future work.

- Though there are biological advantages to use anodized nanostructured titanium alloys for orthopedic applications, several material based issues have to be addressed before they can be offered for clinical trials. For instance, anodically grown oxide on titanium alloys suffer from weak delamination strength between the metallic substrate and the surface oxide. Since implantation of orthopedic implants is an aggressive procedure involving exertion of mechanical loads onto the nanostructured oxide, *i.e.* press fitting to secure the implant into the bone, anodized surface films grown on titanium alloys should be able to withstand the implantation procedure without premature delamination. The delaminated oxide films in the body might potentially act like a wear debris and stimulate immune system and osteoclasts, leading to bone resorption and aseptic failure of the implant. Besides, once nanofeatured oxide film delaminates, the underlying titanium alloy substrate cannot provide the advantages nanofeatured surfaces have to offer. Thus, findings regarding enhanced biocompatibility and bioactivity of the anodized nanotubular surfaces may only be limited to *in vitro* experiments and fail to translate into successful clinical results. Enhancing the delamination strength of the oxide via interacting with a non-protonated polar substance, *i.e.* cyclohexane, would certainly help address this issue [109].

- Depending on the anodization conditions (electrolyte type, concentration, voltage, temperature, and etc.) and post-heat treatment temperature/duration nanofeatures with different physical and chemical properties can be fabricated. Currently, there is not enough information eliciting the effect of different anodized surface morphologies, topographies and chemistries on bone cell response. For instance, it is still not clear if nanotubes or micropits provide best osseointegration. Considering that minute changes in anodization parameters result in different physical and chemical properties for the oxide films, there is no consensus on the optimal physical and chemical properties of surface features to enhance bone cell functions. Besides, studies regarding vascular growth, osteoclast functions and immune cell response on these surfaces are very limited. To successfully translate anodized titanium and titanium alloys for clinical use and benefit from the advantages nanofeatures titanium films have to offer, a better understanding of the cellular response on anodized titanium alloys, followed by detailed *in vivo* large animal studies are required. Only then scientists can have a better understanding of the advantages and potential hazards of using anodized titanium and titanium alloys for orthopedic applications.

## REFERENCES

- [1] Orthopedic implants market analysis, by application (spinal fusion, long bone, foot & ankle, craniomaxillofacial, joint replacement, dental), and segment sorecasts to 2024. (n.d.). Retrieved February 22, 2018, from <https://www.grandviewresearch.com/industry-analysis/orthopedic-implants-market>.
- [2] S. M. Kurtz, Future clinical and economic impact of revision total hip and knee arthroplasty, *The Journal of Bone and Joint Surgery (American)*, 89(2007), pp. 144.
- [3] D. A. Etzioni, J. H. Liu, M. A. Maggard, C. Y. Ko, The aging population and its impact on the surgery workforce, *Annals of Surgery*, 238(2003), pp. 170-177.
- [4] R. D. Ramiah, A. M. Ashmore, E. Whitley, G. C. Banniste, Ten-year life expectancy after primary total hip replacement, *The Journal of Bone and Joint Surgery*, British volume, 89-B(2007), pp.1299-1302.
- [5] V. Sansone, The effects on bone cells of metal ions released from orthopaedic implants, *A review. Clinical Cases In Mineral And Bone Metabolism*, 2013.
- [6] E. Michalesko. (n.d.), Retrieved February 22, 2018, from <http://www.ajrr.net/publications-data/registry-insider-newsletter/newsletter-november-2017/491-ajrr-2017-annual-report-just-released>.
- [7] V. Zwillling, E. Darque-Ceretti, A. Boutry-Forveille, D. David, M. Y. Perrin, M. Aucouturier, Structure and physicochemistry of anodic oxide films on titanium and TA6V alloy, *Surface and Interface Analysis*, 27(1999), pp. 629-637.
- [8] M. Long, H. Rack, Titanium alloys in total joint replacement—a materials science perspective, *Biomaterials*, 19(1998), pp. 1621-1639.

- [9] E. Bütev, Z. Esen, Ş. Bor, Characterization of Ti6Al7Nb alloy foams surface treated in aqueous NaOH and CaCl<sub>2</sub> solutions, *Journal of the Mechanical Behavior of Biomedical Materials*, 60 (2016), pp. 127-138.
- [10] K. Prasad, O. Bazaka, M. Chua, M. Rochford, L. Fedrick, J. Spoor, K. Bazaka, Metallic biomaterials: current challenges and opportunities, *Materials*, 10(2017), pp. 884.
- [11] A. Lavakumar, Concepts in Physical Metallurgy: Concise Lecture Notes. San Rafael, CA: Morgan & Claypool press, 2017.
- [12] S. D. Rogers, D. W. Howie, S. E. Graves, M. J. Pearcy, D. R. Haynes, *In vitro* human monocyte response to wear particles of Titanium alloy containing Vanadium or Niobium, *The Journal of Bone and Joint Surgery*, 79(1997), pp. 311-315.
- [13] K. C. Popat, L. Leoni, C. Grimes, T. A. Desai, Influence of engineered titania nanotubular surfaces on bone cells, *Biomaterials*, 28(2007), pp. 3188-3197.
- [14] L. C. Palmer, C. J. Newcomb, S. R. Kaltz, E. D. Spoerke, S. I. Stupp, Biomimetic systems for hydroxyapatite mineralization inspired by bone and enamel, *Chemical Reviews*, 108(2008), pp. 4754-4783.
- [15] S. J. Liliensiek, P. Nealey, C. J. Murphy, Characterization of endothelial basement membrane nanotopography in rhesus macaque as a Guide for vessel tissue engineering, *Tissue Engineering Part A*, 15(2009), pp. 2643-2651.
- [16] A. Rafieerad, A. Bushroa, A. Hamouda, M. Sarraf, B. Nasiri-Tabrizi, Self-organized TiO<sub>2</sub> nanotube layer on Ti-6Al-7Nb for biomedical application, *Surface and Coatings Technology*, 265 (2015), pp. 24-31.

- [17] J. M. Macak, H. Tsuchiya, L. Taveira, A. Ghicov, P. Schmuki, Self-organized nanotubular oxide layers on Ti-6Al-7Nb and Ti-6Al-4V formed by anodization in  $\text{NH}_4\text{F}$  solutions, *Journal of Biomedical Materials Research Part A*, 75A(2005), pp. 928-933.
- [18] S. Mahshid, M. Goodarzi, M. Askari, A. Ghahramaninezhad, Self-organized titanium oxide nanotubes prepared in phosphate electrolytes: effect of voltage and fluorine concentration, 2010.
- [19] A. Ahmad, E. U. Haq, W. Akhtar, M. Arshad, Z. Ahmad, Synthesis and characterization of titania nanotubes by anodizing of titanium in fluoride containing electrolytes, *Applied Nanoscience*, , 7(2017), pp. 701-710.
- [20] K. Indira, U. K. Mudali, T. Nishimura, N. A. Rajendran, Review on  $\text{TiO}_2$  nanotubes: influence of anodization parameters, formation mechanism, properties, corrosion behavior, and biomedical applications, *Journal of Bio- and Tribo-Corrosion*, 1(2015).
- [21] J. Macak, H. Tsuchiya, A. Ghicov, K. Yasuda, R. Hahn, S. Bauer, P. Schmuki,  $\text{TiO}_2$  nanotubes: self-organized electrochemical formation, properties and applications”, *Current Opinion in Solid State and Materials Science*, 11(2007), pp. 3-18.
- [22] P. Roy, S. Berger, P. Schmuki,  $\text{TiO}_2$  Nanotubes: synthesis and applications, *Angewandte Chemie International Edition*, 50(2011), pp. 2904-2939.
- [23] H. Omidvar, S. Goodarzi, A. Seif, A. R. Azadmehr, Influence of anodization parameters on the morphology of  $\text{TiO}_2$  nanotube arrays, *Superlattices and Microstructures*, 50(2011), pp. 26-39.



- [24] A. L. Escada, R. Z. Nakazato, A. P. Claro, Influence of anodization parameters in the TiO<sub>2</sub> nanotubes formation on Ti-7.5Mo alloy surface for biomedical application, *Materials Research*, 20(2017), pp. 1282-1290.
- [25] D. Regonini, C. Bowen, A. Jaroenworarluck, R. Stevens, A review of growth mechanism, structure and crystallinity of anodized TiO<sub>2</sub> nanotubes, *Materials Science and Engineering: R: Reports*, 74(2013), pp. 377-406.
- [26] X. Feng, J. M. Macak, P. Schmuki, Robust self-organization of oxide nanotubes over a wide pH range, *Chemistry of Materials*, 19(2007), pp. 1534-1536.
- [27] S. Sreekantan, Z. Lockman, R. Hazan, M. Tasbihi, L. K. Tong, A. R. Mohamed, Influence of electrolyte pH on TiO<sub>2</sub> nanotube formation by Ti anodization, *Journal of Alloys and Compounds*, 485(2009), pp. 478-483.
- [28] J. Chen, J. Lin, X. Chen, Self-assembled TiO<sub>2</sub> nanotube arrays with U-shaped profile by controlling anodization temperature, *Journal of Nanomaterials*, 2010, pp. 1-4.
- [29] D. Gong, C. A. Grimes, O. K. Varghese, W. Hu, R. S. Singh, Z. Chen, E. Dickey, Titanium oxide nanotube arrays prepared by anodic oxidation, *Journal of Materials Research*, 16(2001), pp. 3331-3334.
- [30] M. Kulkarni, A. Mazare, P. Schmuki, A. Iglic, Influence of anodization parameters on morphology of TiO<sub>2</sub> nanostructured surfaces, *Advanced Materials Letters*, 7(2016), pp. 23-28.
- [31] V. Zwillig, E. Darque-Ceretti, A. Boutry-Forveille, D. David, M. Y. Perrin, M. Aucouturier, Structure and physicochemistry of anodic oxide films on titanium and TA6V alloy, *Surface and Interface Analysis*, 27(1999), pp. 629-637.
- [32] R. Beranek, H. Hildebrand, P. Schmuki., Self-organized porous titanium oxide prepared in H<sub>2</sub>SO<sub>4</sub>/HF electrolytes, *Electrochemical and Solid-State Letters*, 6(2003).

- [33] J. Chen, J. Lin, X. Chen, Self-assembled TiO<sub>2</sub> nanotube arrays with U-shaped profile by controlling anodization temperature, *Journal of Nanomaterials*, 2010, pp. 1-4.
- [34] Q. Cai, M. Paulose, O. K. Varghese, C. A. Grimes, The effect of electrolyte composition on the fabrication of self-organized titanium oxide nanotube arrays by anodic oxidation, *Journal of Materials Research*, 20(2005), pp. 230-236.
- [35] J. Macak, M. Zlamal, J. Krysa, P. Schmuki, Self-organized TiO<sub>2</sub> nanotube layers as highly efficient photocatalysts, *Small*, 3(2007), pp. 300-304.
- [36] A. Mazare, M. Dilea, D. Ionita, I. Titorencu, V. Trusca, E. Vasile, Changing bioperformance of TiO<sub>2</sub> amorphous nanotubes as an effect of inducing crystallinity, *Bioelectrochemistry*, 87(2012), pp. 124-131.
- [37] A. Kaczmarek, T. Klekiel, E. Krasicka-Cydzik, Fluoride concentration effect on the anodic growth of self-aligned oxide nanotube array on Ti6Al7Nb alloy, *Surface and Interface Analysis*, 42(2010), pp. 510-514.
- [38] I. S. Park, H. J. Oh, T. S. Bae, Bioactivity and generation of anodized nanotubular TiO<sub>2</sub> layer of Ti-6Al-4V alloy in glycerol solution, *Thin Solid Films*, 548(2013), pp. 292-298.
- [39] L. Mohan, C. Anandan, N. Rajendran, Electrochemical behavior and effect of heat treatment on morphology, crystalline structure of self-organized TiO<sub>2</sub> nanotube arrays on Ti-6Al-7Nb for biomedical applications, *Materials Science and Engineering: C*, 50 (2015), pp. 394-401.
- [40] C. Richter, Z. Wu, E. Panaitescu, R. Willey, L. Menon, Ultra-high-aspect-ratio titania nanotubes, *Advanced Materials*, 19(2007), pp. 946-948.

- [41] N. K. Allam, K. Shankar, C. A. Grimes, Photoelectrochemical and water photoelectrolysis properties of ordered TiO<sub>2</sub> nanotubes fabricated by Ti anodization in fluoride-free HCl electrolytes, *Journal of Materials Chemistry*, 18(2008) pp, 2341.
- [42] S. Kim, M. Seong, J. Choi, Rapid breakdown anodization for the preparation of titania nanotubes in halogen-free Acids, *Journal of the Electrochemical Society*, 2015, 162(2015).
- [43] Y. L. Cheong, F. K. Yam, S. W Ng, Z Hassan, S.Ng S, I. M. Low, Fabrication of titanium dioxide nanotubes in fluoride-free electrolyte via rapid breakdown anodization, *Journal of Porous Materials*, 22(2015), pp.1437-1444.
- [44] J. M. Schakenraad, H. J. Busscher, C. R. Wildevuur, J. Arends, The influence of substratum surface free energy on growth and spreading of human fibroblasts in the presence and absence of serum proteins, *Journal of Biomedical Materials Research*, 20(1986), pp. 773-784.
- [45] S. D. Puckett, E. Taylor, T. Raimondo, T. J. Webster, The relationship between the nanostructure of titanium surfaces and bacterial attachment, *Biomaterials*, 31(2010), pp. 706-713.
- [46] L. Wang, M. Jin, Y. Zheng, Y. Guan, X. Lu, J. Luo, Nanotubular surface modification of metallic implants via electrochemical anodization technique, *International Journal of Nanomedicine*, 2014, pp. 4421.
- [47] T. Webster, C. Ergun, R.H. Doremus, R.W. Siegel, R. Bizios, Enhanced functions of osteoblasts on nanophase ceramics, *Biomaterials*, 21(2000), pp.1803-1810.
- [48] T. Webster, J. U. Ejiofor, Increased osteoblast adhesion on nanophase metals: Ti, Ti6Al4V, and CoCrMo, *Biomaterials*, 25(2004), pp. 4731-4739.

- [49] T. Webster, Greater osteoblast and endothelial cell adhesion on nanostructured polyethylene and titanium, *International Journal of Nanomedicine*, 2010, pp. 647.
- [50] W. Ji, P. Han, C. Zhao, Y. Jiang, X. Zhang, Increased osteoblast adhesion on nanophase Ti6Al4V, *Science Bulletin*, 53(2008), pp. 1757-1762.
- [51] K. S. Brammer, S. Oh, C. J. Cobb, L. M. Bjursten, H. V. Heyde, S. Jin, Improved bone-forming functionality on diameter-controlled TiO<sub>2</sub> nanotube surface, *Acta Biomaterialia*, 5(2009), pp. 3215-3223.
- [52] T. Webster, Ross, Anodizing color coded anodized Ti6Al4V medical devices for increasing bone cell functions, *International Journal of Nanomedicine*, 2013, pp.109.
- [53] C. Yao, E. B. Slamovich, T. J. Webster, Enhanced osteoblast functions on anodized titanium with nanotube-like structures, *Journal of Biomedical Materials Research Part A*, 85A(2008), pp.157-166.
- [54] P. Roy, S. Berger, P. Schmuki, TiO<sub>2</sub> Nanotubes: Synthesis and Applications, *Angewandte Chemie International Edition*, 50(2011), pp. 2904-2939.
- [55] A. Tan, B. Pinguan-Murphy, R. Ahmad, S. Akbar, Review of titania nanotubes: Fabrication and cellular response, *Ceramics International*, 38(2012), pp. 4421-4435.
- [56] J. Park, S. Bauer, K. V. Mark, P. Schmuki, Nanosize and vitality: TiO<sub>2</sub> nanotube diameter directs cell fate, *Nano Letters*, 7(2007), pp.1686-1691.
- [57] B. Ercan, K. M. Kummer, K. M. Tarquinio, T. J. Webster, Decreased staphylococcus aureus biofilm growth on anodized nanotubular titanium and the effect of electrical stimulation, *Acta Biomaterialia*, 7(2011), pp. 3003-3012.
- [58] K. S Brammer, S. Oh, J. O. Gallagher, S. Jin, Enhanced cellular mobility guided by TiO<sub>2</sub> nanotube surfaces, *Nano Letters*, 8(2008), pp.786-793.

- [59] W. Yu, Y. Zhang, X. Jiang, F. Zhang, *In vitro* behavior of MC3T3-E1 preosteoblast with different annealing temperature titania nanotubes, *Oral Diseases*, 16(2010), pp. 624-630.
- [60] S. Oh, K. S. Brammer, Y. S. Li, D. Teng, A. J. Engler, S. Chien, S. Jin, Stem cell fate dictated solely by altered nanotube dimension, *Proceedings of the National Academy of Sciences*, 106(2009), pp. 2130-2135.
- [61] K. S. Brammer, S. Oh, C. J. Cobb, L. M. Bjursten, H. V. Heyde, Jin S, Improved bone-forming functionality on diameter-controlled TiO<sub>2</sub> nanotube surface, *Acta Biomaterialia*, 5(2009), pp. 3215-3223.
- [62] K. Malec, J. Goralska, M. Hubalewska-Mazgaj, P. Glowacz, M. Jarosz, P. Brzewski, Effects of nanoporous anodic titanium oxide on human adipose derived stem cells, *International Journal of Nanomedicine*, 11(2016), pp. 5349-5360.
- [63] G. Li, Q. Zhao, H. Tang, G. Li, Y. Chi, Fabrication, characterization and biocompatibility of TiO<sub>2</sub> nanotubes via anodization of Ti6Al7Nb, *Composite Interfaces*, 23(2016), pp. 223-230.
- [64] E. Filova, J. Fojt, M. Kryslova, H. Moravec, L. Joska, L. Bacakova, The diameter of nanotubes formed on Ti-6Al-4V alloy controls the adhesion and differentiation of Saos-2 cells, *International Journal of Nanomedicine*, 2015, pp. 7145.
- [65] J. M. Macak, H. Tsuchiya, L. Taveira, A. Ghicov, and P. Schmuki, Self-organized nanotubular oxide layers on Ti-6Al-7Nb and Ti-6Al-4V formed by anodization in NH<sub>4</sub>F solutions, *J. Biomed. Mater. Res. - Part A*, 75(2005), pp. 928–933.
- [66] I. S. Park, H. J. Oh, and T. S. Bae, Bioactivity and generation of anodized nanotubular TiO<sub>2</sub> layer of Ti-6Al-4V alloy in glycerol solution, *Thin Solid Films*, 548(2013), pp. 292–298.

- [67] A. P. Ross and T. J. Webster, Anodizing color coded anodized Ti6Al4V medical devices for increasing bone cell functions, *Int. J. Nanomedicine*, 8(2013), pp. 109–117.
- [68] K. Ishibashi, R. Yamaguchi, Y. Kimura, and M. Niwano, Fabrication of Titanium Oxide Nanotubes by Rapid and Homogeneous Anodization in Perchloric Acid/Ethanol Mixture, *J. Electrochem. Soc.*, 155(2008), pp. K10.
- [69] Y. L. Cheong, F. K. Yam, S. W. Ng, Z. Hassan, S. S. Ng, and I. M. Low, Fabrication of titanium dioxide nanotubes in fluoride-free electrolyte via rapid breakdown anodization, *J. Porous Mater.*, 22(2015), pp. 1437–1444.
- [70] N. K. Allam, K. Shankar, and C. A. Grimes, Photoelectrochemical and water photoelectrolysis properties of ordered TiO<sub>2</sub> nanotubes fabricated by Ti anodization in fluoride-free HCl electrolytes, *J. Mater. Chem.*, 18(2008), pp. 2341.
- [71] D. Regonini, C. R. Bowen, A. Jaroenworarluck, and R. Stevens, A review of growth mechanism, structure and crystallinity of anodized TiO<sub>2</sub> nanotubes, *Mater. Sci. Eng. R Reports*, 74(2013), pp. 377–406.
- [72] X. Cui *et al.*, Apatite formation on anodized Ti-6Al-4V alloy in simulated body fluid, *Met. Mater. Int.*, 16(2010), pp. 407–412.
- [73] Narayanan, R., Seshadri, S, Phosphoric acid anodization of Ti-6Al-4V Structural and corrosion aspects, *Corrosion Science*, 49(2007), pp.542-558.
- [74] T. Kokubo and H. Takadama, How useful is SBF in predicting in vivo bone bioactivity?, *Biomaterials*, 27(2006), pp. 2907–2915.
- [75] E. Krasicka-Cydzik, Anodic layer formation on titanium and its alloys for biomedical applications, *Titanium Alloys - Towards Achieving Enhanced Properties for Diversified App.*, 2012, pp. 175-200.

- [76] Y. L. Cheong, F. K. Yam, S. W. Ng, Z. Hassan, S. S. Ng, I. M. Low, Fabrication of titanium dioxide nanotubes in fluoride-free electrolyte via rapid breakdown anodization, *J. Porous Mater.*, 22(2015), pp. 1437–1444.
- [77] N. K. Allam, K. Shankar, C. A. Grimes, Photoelectrochemical and water photoelectrolysis properties of ordered TiO<sub>2</sub> nanotubes fabricated by Ti anodization in fluoride-free HCl electrolytes, *J. Mater. Chem.*, 18(2008), pp. 2342-2348.
- [78] E. Panaitescu, C. Richter, L. Menon, A study of titania nanotube synthesis in chloride-ion-containing media, *J. Electrochem. Soc.*, 155(2008), pp. E7-E13.
- [79] J. M. Macak, H. Tsuchiya, L. Taveira, A. Ghicov, P. Schmuki, Self-organized nanotubular oxide layers on Ti-6Al-7Nb and Ti-6Al-4V formed by anodization in NH<sub>4</sub>F solutions, *J. Biomed. Mater. Res. Part A*, 75(2005), pp. 928–933.
- [80] G. T. Burstein, C. Liu, R. M. Souto, S. P. Vines, Origins of pitting corrosion, *Corros. Eng.Sci. and Technol.*, 39(2004), pp. 26-30.
- [81] C. Richter, Z. Wu, E. Panaitescu, R. J. Willey, L. Menon, Ultrahigh-aspect-ratio titania nanotubes, *Adv. Mater.*, 19(2007), pp. 946–948.
- [82] M. V. Popa, Electrochemical deposition of bioactive coatings on Ti and Ti-6Al-4V surfaces, *Surf. Coat. Technol.*, 205 (2011), pp. 4776–4783.
- [83] S Guimond, M. A. Haija, S. Kaya, J. Lu, J. Weissenrieder, S. Shaikhutdinov, J. Sauer, Vanadium oxide surfaces and supported vanadium oxide nanoparticles, *Top. Catal.*, 38(2006), pp. 117-125.
- [84] S. B. Patel, Functionalization and Characterization of CP-Ti and Ti-6Al-4V Surfaces for Biomedical Implants, Dissertation for the Master degree, Chicago: University of Illinois, 2013, pp. 44-67.
- [85] Z. Su, W. Zhou, Formation, microstructures and crystallization of anodic titanium oxide tubular arrays, *J Mater. Chem.*, 19(2009), pp. 2301-2309.

- [86] M. L. Vera, M. R. Rosenberger, C. E. Schvezov, A. E. Ares, Fabrication of TiO<sub>2</sub> crystalline coatings by combining Ti-6Al-4V anodic oxidation and heat treatments, *Int. J. Biomater.*, 2015(2015), pp. 1-9.
- [87] F. López-Huerta, B. Cervantes, O. González, J. Hernández-Torres, L. García-González, R. Vega, A. L. Herrera-May, E. Soto, Biocompatibility and surface properties of TiO<sub>2</sub> thin films Deposited by DC Magnetron Sputtering, *Mater. (Basel)*., 7(2014), pp. 4105–4117.
- [88] B. Cervantes, F. López-Huerta, R. Vega, J. Hernández-Torres, L. García-González, E. Salceda, A. L. Herrera-May, E. Soto, Cytotoxicity Evaluation of Anatase and Rutile TiO<sub>2</sub> Thin Films on CHO-K1 Cells in Vitro, *Mater. (Basel)*., 9(2016), pp. 619.
- [89] Y. Zhang, Y. Han, L. Zhang, Interfacial structure of the firmly adhered TiO<sub>2</sub> nanotube films to titanium fabricated by a modified anodization, *Thin Solid Films*, 583(2015), pp. 151–157.
- [90] The Infrared Spectra of Some Ti-O-Si, Ti-O-Ti and Si-O-Si Compounds. <https://pubs.acs.org/doi/pdf/10.1021/j150555a010>, 2018 (accessed 24 June 2018).
- [91] D. Kong, The influence of fluoride on the physicochemical properties of anodic oxide films formed on titanium surfaces, *Langmuir*, 24(2008), pp. 5324-5331.
- [92] L. Lin, H. Wang, M. Ni, Y. Rui, T.Y. Cheng, C. K. Cheng, X. Pan, G. Li, C. Lin, Enhanced osteointegration of medical titanium implant with surface modifications in micro/nanoscale structures, *J. Orth. Trans.*, 2(2014), pp. 35-42.
- [93] G. B. de Souza de L, G. de Lima, N. K. Kuromoto, P. Soares, C. M. Lepienski, C. E. Foerster, A. Mikowski, Tribo-mechanical characterization of rough, porous and bioactive Ti anodic layers, *J. Mech. Behav. Biomed. Mater.*, 4(2011), pp. 796–806.
- [94] B. S. Smith, S. Yoriya, L. Grissom, C. A. Grimes, K.C. Popat, Hemocompatibility of titania nanotube arrays, *J. Biomed. Mater. Res. - Part A* , 96A(2010), pp. 350-360.



- [95] J. M. Macak, H. Tsuchiya, A. Ghicov, K. Yasuda, R. Hahn, S. Bauher, P. Schmuki., TiO<sub>2</sub> nanotubes: Self-organized electrochemical formation, properties and applications, *Curr. Opin. Solid State Mater. Sci.*, 11(2007), pp. 3-18.
- [96] Y. L. Cheong, F. K. Yam, S. W. Ng, Z. Hassan, S. S. Ng, I. M Low, Fabrication of titanium dioxide nanotubes in fluoride-free electrolyte via rapid breakdown anodization, *J. Porous Mater.*, 22 (2015), pp. 1437–1444.
- [97] R. Hahn, M. Stark, M. S. Killian, P. Schmuki, Photocatalytic properties of in situ doped TiO<sub>2</sub>-nanotubes grown by rapid breakdown anodization, *Catal. Sci. Technol.*, 3(2013), pp. 1765-1770.
- [98] Y. Wei-Qiang, J. Xing-guan, Z. Fu-qiang, X. Ling, The effect of anatase TiO<sub>2</sub> nanotube layers on MC3T3-E1 preosteoblast adhesion, proliferation, and differentiation, *J. Biomed. Mater. Res. Part A*, 94A(2010), pp. 1012-1022.
- [99] L. Wang, M. Jin, Y. Zheng, Y. Guan, X. Lu, J Luo, Nanotubular surface modification of metallic implants via electrochemical anodization technique, *Inter. J. Nanomed*, 9(2014), pp. 4421.
- [100] J. Lincks, B. D. Boyan, C. R. Blanchard, C. H. Lochmann, Y. Liu, D. L. Cochran, D.d. Dean, Z. Schwartz, Response of MG63 osteoblast-like cells to titanium and titanium alloy is dependent on surface roughness and composition, in *The Biomaterials: Silver Jubilee Compendium*, 19(2006), pp. 147–160.
- [101] L. Salou, A. Hoornaert, G. Louarn, P. Layrolle, Enhanced osseointegration of titanium implants with nanostructured surfaces: An experimental study in rabbits, *Acta Biomaterialia*, 11(2015), pp. 494-502.
- [102] S. Puckett, Select nanofabricated titanium materials for enhancing bone and skin growth of intraosseous transcutaneous amputation prostheses, Dissertation for the Doctoral Degree, Rhode Island: Brown University, 2011, pp. 286-300.

- [103] RV. Chernozem, , M A Surmeneva, R. A Surmenev, Influence of Anodization Time and Voltage on the Parameters of TiO<sub>2</sub> Nanotubes, IOP Conference Series: Materials Science and Engineering, 116(2016), pp. 012025.
- [104] Serhat Ün N., Development of Sol-Gel Derived Hydroxyapatite-Titania Coatings, Master Thesis, Middle East Technical University, Metallurgical and Materials Engineering, Ankara, 2008.
- [105] C. Bayram, Ortopedik İmplantların Nanoteknolojik Yaklaşımlarla Fonksiyonelleştirilmesi, Doktora Tezi, Hacettepe Üniversitesi, Nanoteknoloji ve Nanotıp Ana Bilim Dalı, Ankara, 2013.
- [106] Y.Chou, W. Chiou, Y. Xu, J. Dunn, B. M. Wu, The Effect of pH on the Structural Evolution of Accelerated Biomimetic Apatite, *Biomaterials*, 25(2004), pp. 5323-5331,
- [107] Kıcır K., Elektroforetik Biriktirme Metodu ile Yüzeyi Modifiye Titanyum İmplantların Hazırlanması ve Karakterizasyonu, Yüksek Lisans Tezi, Hacettepe Üniversitesi, Nanoteknoloji ve Nanotıp Ana Bilim Dalı, Ankara, 2013.
- [108] H. Dong, Tolou S., C. ChangKyoung, L. Seong-Hyuk and C. Friedrich, Wettability Changes of TiO<sub>2</sub> Nanotube Surfaces, *IOP Science*, 22(31), 2011.
- [109] M. Zhao, J. Li, Y. Li, J. Wang, Y. Zuo, J. Jiang, H. Wang, Gradient control of the adhesive force between Ti/TiO<sub>2</sub> nanotubular arrays fabricated by anodization, *Scientific Reports*, 4(2014).

## Copyright Transfer Statement

Copyright-owner: Batur Erkan Tel/Fax: +92(312)2102512

Passport or ID Number S 02330330 E-mail: baerkan@netu.edu.tr

Address (Post code): Univ. Giteker Mah. D. Kurupinar Bul. No:1 B2001022 0605 Ankara Turkey

The paper's title: Modulation of Titanium Alloys for Orthopedic Applications

Whereas the paper above (English language version, hereinafter referred to as the Paper) of Copyright-owner is to be published by Higher Education Press Limited Company (hereinafter referred to as the Publisher) in the English academic journal *Frontiers of Chemical Science and Engineering* (hereinafter referred to as the Journal), the following statements have been reached by Copyright-owner:

**Article 1** Copyright-owner agrees to assign to the Publisher (with no contribution fee from the Publisher to Copyright-owner) the exclusive, assignable and sublicensable rights, unlimited in time and territory, to compile, reproduce, publish, distribute, translate, transmit, make available and archive the paper, including abstracts thereof, in all forms and media of expression now known or developed in the future, including pre- and reprints, translations, photographic reproductions and microform. The Publisher may use the article in whole or in part in electronic form, such as use in databases or data networks for display, print or download to stationary or portable devices. This includes interactive and multimedia use and the right to alter the article to the extent necessary for such use.

**Article 2** Copyright-owner warrants that the Paper is Copyright-owner's original work and has not been published previously anywhere, in any language and form, and promises not to publish this paper elsewhere later in any language and form. Copyright-owner warrants that the paper infringes no copyrights and legal rights of any third party, and no license from or payments to a third party is required to publish the article. If excerpts from copyrighted works, tables, figures, graphs or other such materials are included, Copyright-owner will obtain written permission from the copyright owners and show credit to the sources in the manuscript. Copyright-owner warrants the possession of the copyright of the Paper and the right to assign the aforesaid right to the Publisher through the Statement. If the Paper is of joint authorship, Copyright-owner shall be authorized by any additional copyright owner to assign the aforesaid right and sign the Statement with the Publisher. The performance of the contractual obligations by the Publisher to Copyright-owner shall be deemed having performed the contractual obligations to all the copyright owners, and whereby the Publisher shall be exempt from disputes with any other copyright owners of the paper. Copyright-owner warrants that he/she will not post the Publisher's final version of the Paper on public websites.

**Article 3** In order to tally with the requirements related to the publication and the literature index systems for papers, Copyright-owner authorizes the Publisher to make necessary supplements and modifications to the abstracts, keywords, references and texts of the paper.

**Article 4** In respect of figures and graphs wherein, with graphical abstract included, Copyright-owner agrees to transfer the exclusive right to the Publisher. Without written permission of the Publisher, Copyright-owner shall make no use of the illustrations made by the Publisher for no purposes other than that of the Journal.

**Article 5** Prior versions of the article published on non-commercial pre-print servers like arXiv.org can remain on these servers and/or can be updated with Copyright-owner's accepted version. Copyright-owner may self-archive Copyright-owner-created version of his/her Paper on his/her own website and/or in his/her institutional repository. He/she may also deposit this version on his/her funder's or funder's designated repository at the funder's request or as a result of a legal obligation, provided it is not made publicly available until 12 months after official publication. The final published version (in pdf or html/xml format) cannot be used for these purposes. In all these cases acknowledgement needs to be given to the final publication and a link to the published article on the Publisher's website should be inserted.

Copyright-owner retains the right to use his/her article for his/her further scientific career by including the final published journal article in other publications such as dissertations and postdoctoral qualifications provided acknowledgement is given to the original source of publication.

**Article 6** This Statement shall be effective as of the date of its signature.

Copyright-owner (signature): Batur Erkan

Date: 13.06.2018



# GAZİ ÜNİVERSİTESİ MÜHENDİSLİK-MİMARLIK FAKÜLTESİ DERGİSİ

## Telif Hakkı Devir Formu

Biz aşağıda gerekli bilgileri bulunan,

[Yazarların Adı:] *Merve İzmir, Yiğithan Tufan, Batır Ercan*

tarafımızdan yazılmış,

[Makale Adı:] *Anodize TIBALININ simüle edilmiş vücut  
sıvısı ile etkileşimi*

başlıklı makale içeriği, sunduğu sonuçları ve yorumları konusunda, Gazi Üniversitesi Mühendislik-Mimarlık Fakültesi Dergisi Editörlüğü'nün hiç bir sorumluluk taşımadığını kabul ederiz.

Sunduğumuz makalenin orijinal olduğunu; herhangi bir başka dergiye yayınlanmak üzere verilmediğini; daha önce yayınlanmadığını; eğer tümüyle ya da bir bölümü yayınlandı ise yukarıda adı geçen dergide yayınlanabilmesi için gerekli her türlü iznin alındığını ve orijinal telif hakkı devri formu ile birlikte Gazi Üniversitesi Mühendislik-Mimarlık Fakültesi Dergisi Editörlüğü'ne gönderildiğini garanti ederiz.

Makalenin telif hakkından feragat etmeyi kabul ederek sorumluluğu üstlenir ve imza ederiz. Bu vesileyle makalenin telif hakkı Gazi Üniversitesi Mühendislik-Mimarlık Fakültesi'ne devredilmiştir. Mühendislik-Mimarlık Fakültesi Dergisi Editörlüğü makalenin yayınlanabilmesi konusunda yetkili kılınmıştır. Bununla birlikte yazarların aşağıdaki hakları saklıdır:

Aşağıdaki bütün durumlarda makalenin Gazi Üniversitesi Mühendislik-Mimarlık Fakültesi Dergisi tarafından yayınlandığına dair tam olarak referans verilmelidir.

1. Telif Hakkı dışında kalan patent v.b. bütün tescil edilmiş haklar.
2. Yazarın gelecekteki kitaplar ve dersler gibi çalışmalarında; makalenin tümü yada bir bölümünü ücret ödemeksizin kullanma hakkı.
3. Makaleyi satmamak koşulu ile kendi amaçları için çoğaltma hakkı.

**Bütün yazarlar tarafından imzalanmak üzere:**

<u>Yazarın Adı ve Soyadı</u>	<u>İmzası</u>	<u>Tarih</u>
1 <i>Merve İzmir</i>	<i>M. İzmir</i>	<i>21.07.2017</i>
2 <i>Batır Ercan</i>	<i>Batır Ercan</i>	<i>21.07.2017</i>
3 <i>Yiğithan Tufan</i>	<i>Yiğithan Tufan</i>	<i>21.07.2017</i>
4		
5		
6		

**NOT:** Eksik imza durumunda sorumluluk imzalayan yazarlara aittir. Lütfen formu doldurunuz, çıktı alıp imzalayınız ve taratarak sisteme pdf olarak yükleyiniz.